A Set of Regioselective *O*-Methyltransferases Gives Rise to the Complex Pattern of Methoxylated Flavones in Sweet Basil[1][C][W][OA]

Anna Berim, David C. Hyatt, and David R. Gang*

Institute of Biological Chemistry, Washington State University, Pullman, Washington 99164

Polymethoxylated flavonoids occur in a number of plant families, including the Lamiaceae. To date, the metabolic pathways giving rise to the diversity of these compounds have not been studied. Analysis of our expressed sequence tag database for four sweet basil (*Ocimum basilicum*) lines afforded identification of candidate flavonoid *O*-methyltransferase genes. Recombinant proteins displayed distinct substrate preferences and product specificities that can account for all detected 7-/6-/4′-methylated, 8-unsubstituted flavones. Their biochemical specialization revealed only certain metabolic routes to be highly favorable and therefore likely in vivo. Flavonoid *O*-methyltransferases catalyzing 4′- and 6-*O*-methylations shared high identity (approximately 90%), indicating that subtle sequence changes led to functional differentiation. Structure homology modeling suggested the involvement of several amino acid residues in defining the proteins' stringent regioselectivities. The roles of these individual residues were confirmed by site-directed mutagenesis, revealing two discrete mechanisms as a basis for the switch between 6- and 4′-*O*-methylation of two different substrates. These findings delineate major pathways in a large segment of the flavone metabolic network and provide a foundation for its further elucidation.

The production of "secondary" or specialized metabolites is part of the chemical defense, ecological adaptation, and signaling mechanisms of plants (Wink, 2008; Pichersky and Lewinsohn, 2011). Starting from common precursors, plants produce arrays of specialized compounds using several recurring strategies, including transfer of acyl, sugar, or methyl moieties, often requiring prior hydroxylation steps. Such modifications change not only the physicochemical but also the physiological properties of metabolites (Gang, 2005; Wink, 2008; Pichersky and Lewinsohn, 2011). *O*-Methylation is found in nearly all classes of specialized metabolites, such as alkaloids, phenylpropanoids, and flavonoids (Gang, 2005; Roje, 2006), and is an ancient method of modifying metabolites in plants. For example, the wide distribution of polymethoxylated flavonoids (PMFs) that are well known from the Lamiaceae, Asteraceae, and Rutaceae families (Wollenweber and Dietz, 1981; Emerenciano et al., 1987) but also occur in ferns (Cooper-Driver, 1980; Wollenweber, 1989) attests to the ancient origin of this biosynthetic capacity. Learning how arrays of such compounds are produced is a critical component to developing an understanding of how plants evolve new biosynthetic capacities.

Sweet basil (*Ocimum basilicum*) is a culinary herb belonging to the mint family that also serves as a model system to investigate specialized metabolism in specific cell types in plants. The volatile compounds defining the flavor of basil are produced by the secretory cells and then stored in the oil cavity under the elevated cuticle of the peltate glandular trichomes on the leaf surface (Werker et al., 1993; Gang et al., 2001). Basil also produces PMFs, whose occurrence and distribution in a number of basil cultivars have been studied in detail (Xaasan et al., 1980; Grayer et al., 1996, 2000, 2001; Vieira et al., 2003). Whereas the total PMF amount is probably controlled by the activity of early phenylpropanoid-acetate pathway enzymes, the relative amounts of compounds differing from each other by a methyl or a methoxyl group depend on the late, "decorative" steps, such as 6-, 7-, 8-, 3′-, or 4′-methylations and 6-, 8-, or 3′-hydroxylations. Nothing is known about the flavonoid 6- and 8-hydroxylases in the Lamiaceae, while flavonoid *O*-methyltransferases (FOMTs) from this plant family have received some attention. Five FOMTs from peppermint (*Mentha* × *piperita*) were used for in vivo diversification studies (Willits et al., 2004). However, due to the intended biotechnological application in that study, the potential substrates chosen represented a broad range of flavonoid aglycones rather than physiologically relevant compounds. The studied *O*-methyltransferases (OMTs) methylated both unmethylated and monomethylated

[1] This work was supported by the Department of Energy - Biological and Environmental Research program (grant no. DE–SC0001728 to D.R.G.).

* Corresponding author; e-mail gangd@wsu.edu.

The author responsible for distribution of materials integral to the findings presented in this article in accordance with the policy described in the Instructions for Authors (www.plantphysiol.org) is: David R. Gang (gangd@wsu.edu).

[C] Some figures in this article are displayed in color online but in black and white in the print edition.

[W] The online version of this article contains Web-only data.

[OA] Open Access articles can be viewed online without a subscription.

www.plantphysiol.org/cgi/doi/10.1104/pp.112.204164

flavonoids, prompting a suggestion that the methylation order may not be essential in that plant. Thus, neither the architecture of the PMF network in the mint family nor the factors critical to the production of species-specific PMF profiles and increase of their diversity have been identified.

In this study, we investigated methylation processes leading from apigenin, a common early flavone, to salvigenin (SALV), its 6-hydroxylated, 6,7,4′-trimethylated derivative. Detailed characterization of the major FOMTs derived from a basil trichome EST database suggested that they play dedicated roles in vivo, allowing us to propose the most favorable metabolic routes and to predict the key intermediates in a large segment of the network. Structural studies disclosed how very subtle changes lead to a switch between the 4′- and 6-OMT regioselectivity and two distinct mechanisms affecting this switch. Integration of the biochemical with metabolic and transcript data supported the designated functions for individual FOMTs.

RESULTS

Choice of Basil Lines for an Investigation of Flavone Biosynthesis

Extracts from four standard sweet basil lines (EMX-1, Sweet Dani [SD], SW, and MC; Gang et al., 2001; Iijima et al., 2004; Kapteyn et al., 2007; Xie et al., 2008) contained the major flavonoids known in this species (Grayer et al., 1996, 2001), with SALV and nevadensin (NEV; Fig. 1) being most abundant. Total flavonoid amounts and abundances of putative intermediates were significantly higher in lines SD and EMX-1 compared with SW and MC, while the overall profiles were not identical (Fig. 2A). Lines EMX-1 and SD, therefore, were chosen for further study.

A previous investigation indicated that flavonoids are stored in the subcuticular space of peltate glands in peppermint (Voirin et al., 1993). Therefore, we used stretched glass capillaries to collect the "oil" from the subcuticular space of sets of 150 randomly chosen peltate glands of an approximately 3-cm-long SD or EMX-1 leaf and compared the nonvolatiles in this oil with the flavone profile in the intact second leaf of the leaf pair (Fig. 2, B and C). Major flavonoids found in leaf extracts, such as the flavones SALV, NEV, gardenin B (GARD B), 8-hydroxysalvigenin (8-OH-SALV), cirsimaritin (CIRM), ladanein (LAD), and apigenin-7,4′-dimethyl ether (API-diMe; for structures, see Fig. 1), were easily detectable in these microextracts from trichomes. Given the small number of trichomes collected, the abundance of flavones in the oil seems very high, implying directed accumulation in this compartment (Supplemental Fig. S1, A–D). In comparison, rosmarinic acid, a relatively hydrophilic phenolic compound abundant in leaf extracts, was barely detectable in the collected oil and thus is likely to be equally distributed in the leaf tissue (Supplemental Fig. S1, E–H). The relative amounts of individual flavones in trichome extracts do not exactly mirror the leaf PMF profile (Fig. 2, B and C). Several consistent trends, such as lower relative abundances of pilosin (PIL; Fig. 1), CIRM, and LAD, could indicate a partitioning into a different location (e.g. secretory cells, leaf surface, or mesophyll) for specific PMFs. Alternatively, these discrepancies could be due to variable flavone blends in individual trichomes (e.g. according to their location on the leaf, as was observed for terpenes in peppermint; Maffei et al., 1989). However, random collection of five separate replicate sets of trichomes for each plant yielded highly consistent results and indicates that such variations are likely to be minor. Overall, our results suggest that the majority of the PMFs are primarily if not exclusively stored in the subcuticular oil of the trichomes. These findings show that the glandular trichome system is an appropriate tool for the investigation of the PMF metabolic network.

In Silico Analysis of Candidate Basil FOMTs

While both cation-dependent and non-cation-dependent OMTs (Noel et al., 2003) are represented by numerous contigs in our sweet basil EST database (Gang et al., 2001), the more abundant and diverse group, the non-Mg^{2+}-dependent OMTs, was previously reported to encode FOMTs (Willits et al., 2004). BLAST searches using a peppermint F7OMT protein sequence revealed several candidate F7OMTs from basil. One of the best matches was subsequently used to perform a BLAST search against the EST database. The resulting group is composed of 15 contigs, three of them representing full-length transcripts. The two most abundant putative F7OMT contigs (termed ObFOMT1 and ObFOMT2 and shown in Fig. 3, which will be discussed further below) contain ESTs from all four basil lines, are among the most highly expressed genes in our libraries, and are 94% identical. The remaining 13 polypeptides encoded by minor contigs share 98% to 100% identity with one of the major F7OMTs. The identity of these proteins with the peppermint F7OMT amounted to less than 68%. For comparison, many methyltransferases with conserved functions, such as caffeic acid OMTs, often share more than 80% identity across the plant kingdom.

We followed an analogous strategy to identify the proteins engendering the 4′-*O*-methylations, yielding 20 contigs, with one of them full length and three missing just two to three amino acids at the N terminus. The putative F4′OMT subfamily is more diverse than the F7OMTs, with identities between individual proteins ranging from 87% to 100%. Again, the two most abundant contigs, termed ObFOMT3 and ObFOMT4 (Fig. 3), seemed to represent two clades of the F4′OMT subfamily. Whereas numerous minor contigs were more than 96% identical to one of the major contigs, two contigs stood out by having a lower level of identity to ObFOMT3 or ObFOMT4. The protein termed ObFOMT5 and encoded by a contig with 28 ESTs is 92%

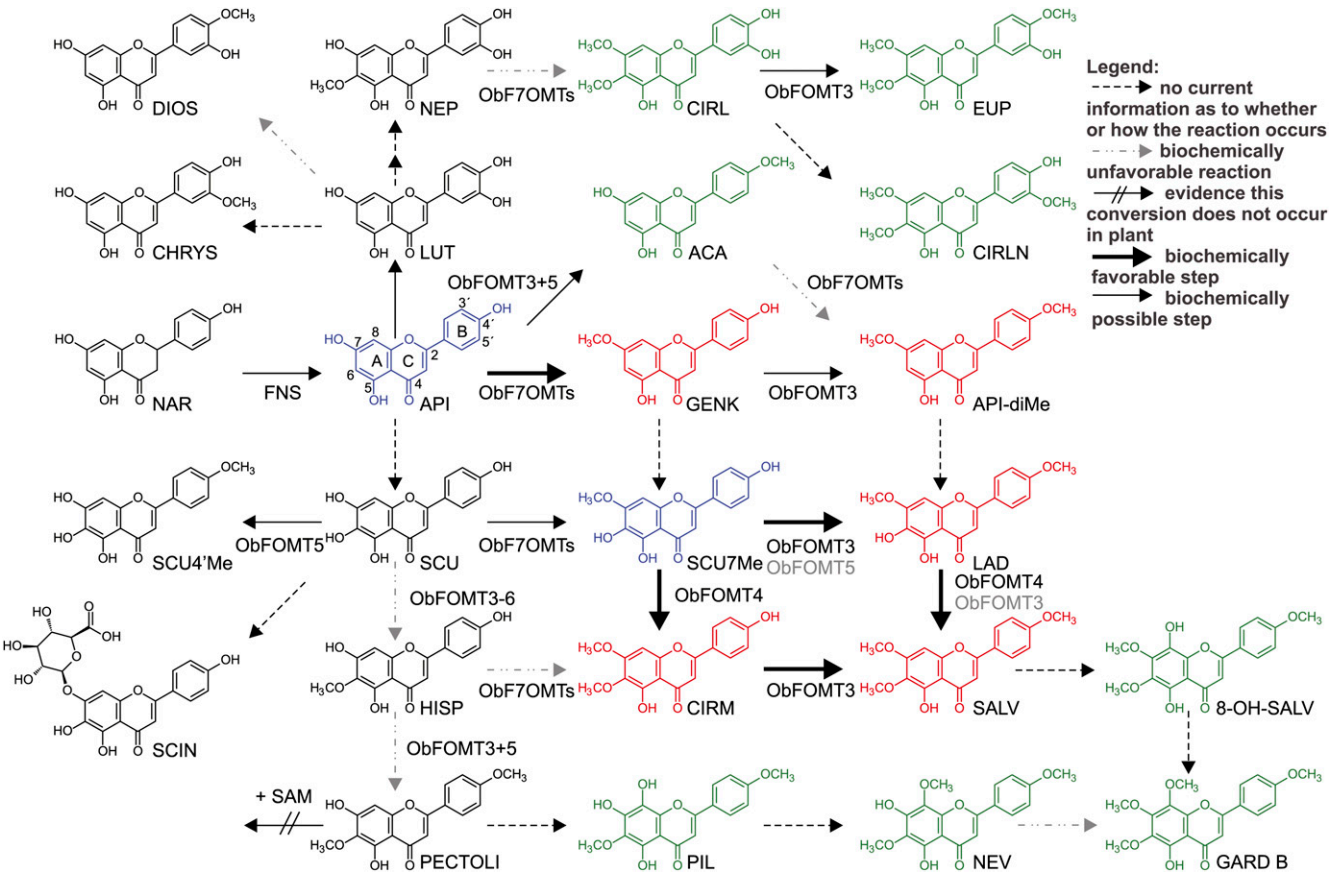

Figure 1. Overview of flavones used as substrates and their positions in the metabolic network in basil, with a focus on steps elucidated in this paper. Color code: green (CIRL, EUP, ACA, cirsilineol [CIRLN], 8-OH-SALV, GARD B, NEV, PIL), accumulated but less relevant in this study; red (GENK, API-diMe, LAD, CIRM, SALV), accumulated in appreciable amounts and relevant to this study; blue (API, SCU7Me), key intermediates suggested by this work. Flavonoid backbone numbering and ring nomenclature are indicated on the API structure. For arrow codes, see key at top right. 7-*O*-Methylation of luteolin is not indicated for space reasons, but it is likely to occur.

identical to ObFOMT3, whereas the protein ObFOMT6, encoded by a very minor (two ESTs) contig, is 92.6% identical to ObFOMT4 (Fig. 3; Supplemental Table S1). Because the activities and substrate preferences of non-Mg^{2+}-dependent *O*-methyltransferases have been shown to switch dramatically by a change in just a few amino acids in several instances (Frick and Kutchan, 1999; Wang and Pichersky, 1999; Frick et al., 2001; Gang et al., 2002; Scalliet et al., 2008; Joe et al., 2010), we chose to study these six putative FOMTs in detail.

Functional Expression and Biochemical Characterization of F7OMTs

The recombinant proteins of all six FOMTs chosen for further characterization were produced in *Escherichia coli*. An N-terminally fused 6× His tag facilitated their purification to near homogeneity (Supplemental Fig. S2). Both basil F7OMTs accepted a broad range of substrates including flavonols such as kaempferol and quercetin, thus being similar to peppermint F7OMTs (Willits et al., 2004). Because basil is only known to accumulate lipophilic flavonoids lacking the 3-hydroxyl moiety (Grayer et al., 1996, 2001; Vieira et al., 2003), we collected physiologically relevant compounds (flavanones and flavones; for a list of trivial, abbreviated, and International Union of Pure and Applied Chemistry names of the flavonoids used in this study, see Supplemental Table S2), including some produced using our FOMTs, and offered them to both F7OMTs. As judged by relative activities at high flavone concentration (100 μM), both ObFOMT1 and ObFOMT2 prefer apigenin (API) and luteolin (LUT) to scutellarein (SCU; for structures, see Fig. 1; Table I). However, kinetic parameters revealed much higher catalytic efficiency (k_{cat}/K_m) of both F7OMTs with API than with LUT and even more so with SCU (Table II).

Within our substrate screen, we noted a striking difference between the relative activities with SCU, a fairly good substrate, and its 6-*O*-methylated derivative hispidulin (HISP; Fig. 1), which is barely methylated by both F7OMTs (Table I). These data are important

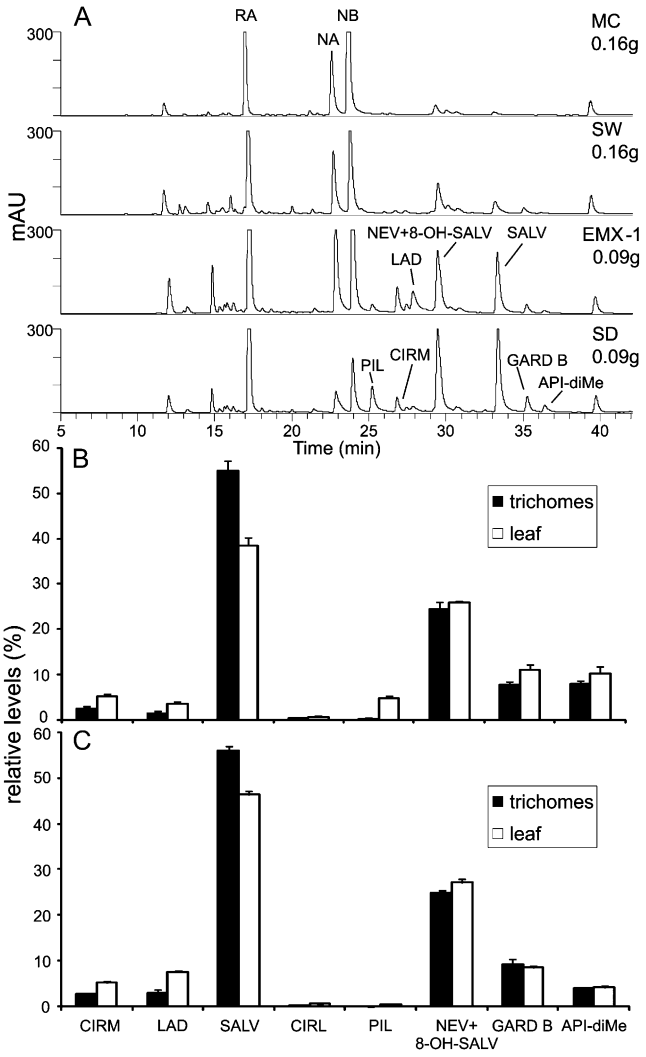

Figure 2. Flavones in sweet basil lines and their localization. A, Representative UV_{335} traces of extracts from four basil lines. Peak labels refer to the flavone designations in Figure 1. Peaks labeled RA, NA, and NB are rosmarinic acid and nepetoidins A and B, respectively. The key on the right indicates basil lines and fresh weight of ground tissue (sixth leaf pair from seven-leaf-pair stage plants) used for extraction using an identical procedure for all lines described in "Materials and Methods." mAU, Milliabsorbance units. B and C, Relative abundances of major flavones in directly collected essential oil versus leaf extracts from lines SD (B) and EMX-1 (C). Total mass signal for the compounds shown was set as 100%. 8-OH-SALV and NEV were not separated and were quantified as one compound. Results are means ± SE from five biological replicates.

for our mapping of metabolic routes in vivo, as they suggest that, at least with these two F7OMTs, 7-*O*-methylation has to precede the 6-*O*-methylation, and if the latter occurs before the former, the products are potentially diverted into a branch leading to compounds like NEV carrying a free 7-hydroxyl group.

The affinities of ObFOMT1 and ObFOMT2 were quite high for API and for the methyl donor, *S*-adenosylmethionine (SAM), as reflected by the low apparent K_m (Table II). The respective demethylated product, *S*-adenosylhomocysteine (SAH), inhibits the reaction by 32.2% (ObFOMT1) and 27.7% (ObFOMT2) when supplied at one-half concentration of SAM (100 μM). Competitive inhibition by SAH is a common feature of *O*-methyltransferases (Clarke and Banfield, 2001). Some product inhibition is also exerted by 10 μM

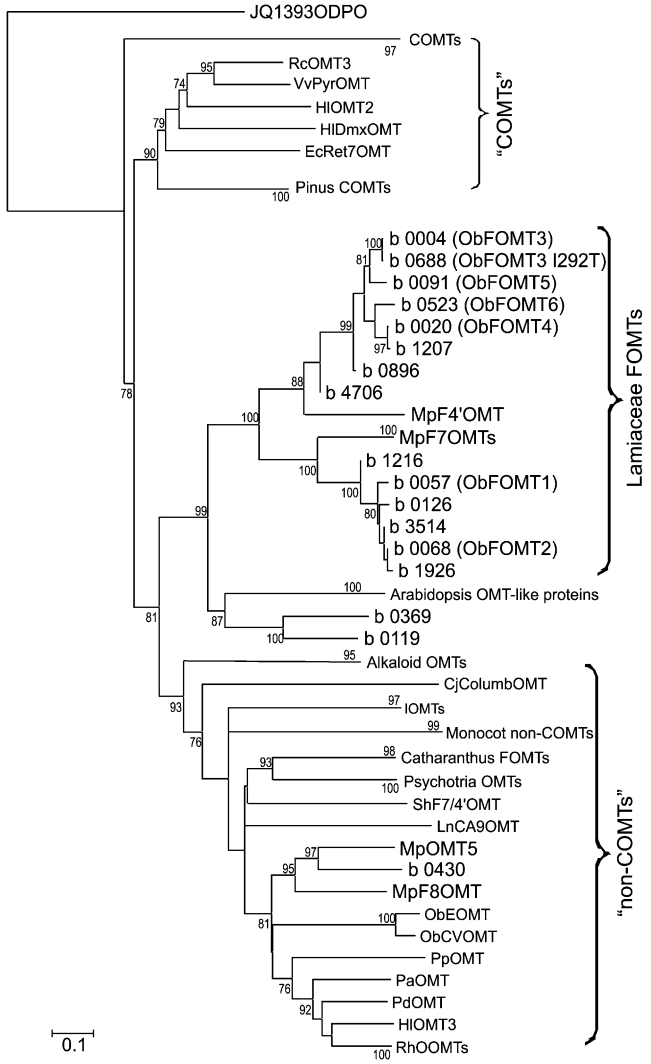

Figure 3. Similarity tree of plant OMTs. Relationships of basil class II OMTs (Ibrahim et al., 1998) to other published OMTs of this class were inferred using the neighbor-joining method (Saitou and Nei, 1987). Only bootstrap values greater than 70% are presented. Bootstrap values next to branch labels refer to the node at the base of a compressed subtree. Scale is in substitutions per amino acid. Branch labels of the type b xxxx (where xxxx indicates designations containing four digits) are the contig numbers in our basil EST database. The compressed COMTs (caffeic acid, or catechol OMTs) branch contains numerous published flavonoid 3′- and 3′/5′-OMTs. For protein designations and accession numbers, including those in selected compressed branches, see "Materials and Methods." MEGA5 (Tamura et al., 2011) was used for tree construction. Outgroup JQ1393ODPO is an *O*-demethylpuromycin OMT from *S. anulatus*.

Table I. *Overview of FOMT activities relative to turnover with the best substrate under linear, optimized conditions*

Values for 100% (nkat mg^{-1} protein) are as follows: 2.57 (FOMT1), 1.21 (FOMT2), 2.15 (FOMT3), 3.51 (FOMT4), 1.66 (FOMT5), 1.03 (FOMT6), 1.87 (FOMT3 S109C/A111T/G181S), 1.30 (FOMT5 C109S/T111A/S181G), and 2.16 (FOMT3 I292T). Results are means of triplicate experiments. Values for two best substrates are in boldface. –, Not measured (not a relevant substrate).

Substrate	F7OMTs		F6/4′OMTs				F6/4′OMT Mutants		
	ObFOMT1	ObFOMT2	ObFOMT3	ObFOMT4	ObFOMT5	ObFOMT6	ObFOMT3 I292T	ObFOMT3 S109C/A111T/G181S	ObFOMT5 C109S/T111A/S181G
API	**92.39**	**91.76**	4.73	0.12	24.09	1.08	21.11	8.90	5.28
LUT	**100**	**100**	0.30	0.25	1.92	2.42	2.83	0.58	0.04
SCU	56.83	51.86	2.59	2.85	7.68	3.25	3.39	4.39	2.18
HISP	3.15	4.53	20.53	0.51	8.39	9.02	8.33	8.20	20.17
NAR	29.32	35.13	0.79	0.07	5.17	0.86	2.86	0.29	1.18
CHRYS	43.00	32.29	0.62	4.91	0.92	45.83	5.09	0.18	1.05
DIOS	23.99	10.71	–	–	–	–	–	–	–
ACA	43.21	23.63	–	–	–	–	–	–	–
SCU4′Me	10.86	10.49	3.21	5.01	3.67	3.70	3.87	4.66	3.76
NEP	1.07	4.97	2.65	0.18	3.42	7.89	4.75	1.19	2.93
PECTOLI	0.27	0.26	–	–	–	–	–	–	–
NEV	3.61	1.76	–	–	–	–	–	–	–
SCU7Me	–	–	**100**	**82.13**	**100**	**100**	**80.93**	**100**	**93.38**
CIRM	–	–	**96.85**	0.38	**54.50**	6.63	**100**	**52.3**	**100**
LAD	–	–	17.06	**100**	0.93	**93.14**	20.92	1.47	11.80
NAR7Me	–	–	4.63	1.14	23.45	2.70	32.11	25.15	7.02
CIRL	–	–	13.95	0.33	6.92	17.76	6.88	4.33	11.64
GENK	–	–	28.24	0.62	32.23	1.42	32.65	38.84	26.48
SCIN	–	–	4.95	1.70	3.35	3.6	5.63	7.25	6.31

genkwanin (GENK), which reduced the *O*-methylation of 10 μM API by 22.5% (ObFOMT1) and 7.1% (ObFOMT2). Both flavonoid 7-*O*-methyltransferases studied possessed very similar properties. The possibility of their temporal/spatial complementarity is addressed below. Because the intermediate occurrence of LUT, SCU, and above all API is very likely, it appears that the latter may serve as the natural substrate for both basil F7OMTs.

Functional Expression and Biochemical Characterization of F4′OMTs (F6/4′OMTs)

All common flavones were methylated by the putative F4′OMTs under long incubation times with excess protein ("max" reactions). However, analysis of products from *O*-methylation of SCU, the simplest 6-hydroxylated flavone, exposed distinct behavior between the four proteins. ObFOMT5 carried out both 6- and 4′-*O*-methylations, whereas ObFOMT3 mostly yielded HISP and smaller amounts of scutellarein-4′-methyl ether (SCU4′Me; Fig. 1). ObFOMT4 and ObFOMT6 only acted as 6-OMTs. In max reactions, three of the four proteins converted the monomethyl ethers of SCU into its 6,4′-dimethyl ether, pectolinarigenin (PECTOLI; Fig. 1). Only with ObFOMT4 did the reaction virtually stop after the first step (Supplemental Fig. S3A, traces 1, 3, 6, and 7).

Another substrate that the four F6/4′OMTs acted differentially upon was scutellarein-7-methyl ether (SCU7Me). Whereas ObFOMT5 yielded almost exclusively the 4′-*O*-methylation product LAD next to minuscule amounts of CIRM, ObFOMT3 almost immediately converted what little it made of CIRM into SALV. Therefore, the regioselectivity of these two FOMTs was altered compared with the products obtained with SCU. Longer incubation with SCU7Me resulted in complete 6- and 4′-*O*-methylation and thus SALV as a final product with ObFOMT3, ObFOMT5, and ObFOMT6. Time-course monitoring indicated that LAD was a better substrate for ObFOMT3 than for ObFOMT5, as the latter only started methylating LAD when very little SCU7Me was left. This is in line with the relative turnover rates of ObFOMT3 and ObFOMT5 with LAD (Table I). Only ObFOMT4 acted strictly as a 6-OMT and seemed unable to carry out the subsequent 4′-methylation of CIRM (Supplemental Fig. S3B). This distinct activity of highly similar proteins with SCU and SCU7Me clearly called for an investigation of structural elements causing the differences (see below).

Unexpectedly, all studied F6/4′OMTs are capable of methylating scutellarein-7-*O*-glucuronide (SCIN). This implies that their substrate-binding sites must have a way to accommodate the bulky sugar acid residue at position 7 rather than the smaller hydroxyl or a more lipophilic methoxyl group. All four F6/4′OMTs prefer a 6-OH residue as methyl group acceptor with SCIN (Supplemental Fig. S4). Subsequent 4′-*O*-methylation was detectable only with ObFOMT3 as catalyst, but at a negligible rate. If the 7-glucuronide (or similar glycoconjugate) indeed occurs as an intermediate in planta, the sugar moiety would have to be cleaved off after the 6-*O*-methylation in order for the 4′-methyl group to be introduced.

Table II. *Kinetic properties of ObFOMT1 to -6 with their best substrates and SAM*

Results are means of three independent experiments ± SE. Only hyperbolic parts of the curves were used for estimating kinetic parameters.

FOMT Group	FOMT	Substrate	K_m	k_{cat}	k_{cat}/K_m
				$s^{-1} \times 10^{-3}$	$\mu M^{-1}\ s^{-1}$
F7OMTs	ObFOMT1	API	32 ± 5.1 nM	91 ± 1.2	2.81
		LUT	240 ± 12 nM	100 ± 4.3	0.43
		SCU	580 ± 31 nM	47 ± 0.2	0.08
		SAM	2.5 ± 0.2 μM		
	ObFOMT2	API	59 ± 10 nM	43 ± 2.1	0.73
		LUT	250 ± 10 nM	49 ± 6.6	0.20
		SCU	250 ± 10 nM	29 ± 4.5	0.12
		SAM	1.9 ± 0.2 μM		
F6/4′OMTs	ObFOMT3	SCU7Me	410 ± 43 nM	85 ± 5	0.21
		CIRM	42 ± 4.2 nM	98 ± 2.4	2.32
		GENK	130 ± 15 nM[a]	57 ± 2.2	0.44
		SAM	36 ± 0.6 μM		
	ObFOMT4	SCU7Me	98 ± 15 nM	130 ± 5.8	1.28
		LAD	54 ± 6 nM	140 ± 12	2.55
		SAM	21 ± 2.0 μM		
	ObFOMT5	SCU7Me	36 ± 4.0 nM	66 ± 5.2	1.81
		CIRM	87 ± 4.7 nM	50 ± 1.8	0.58
		GENK	130 ± 16 nM[b]	72 ± 1.3	0.55
		SAM	41 ± 3.7 μM		
	ObFOMT6	SCU7Me	110 ± 14 nM	41 ± 0.8	0.39
		LAD	36 ± 4.5 nM	29 ± 0.53	0.80
		SAM	78 ± 7.8 μM		

[a]Substrate inhibition at concentration greater than 2.5 μM. [b]Substrate inhibition at concentration greater than 10 μM.

The final overview of relative activities with relevant collected substrates revealed that all four F6/4′OMTs performed best with partially methylated flavones (Table I). Strong and distinct preference of one acceptor moiety allowed the grouping together of ObFOMT4 and ObFOMT6 as predominantly 6-*O*-methyltransferases. On the other hand, ObFOMT3 and ObFOMT5 could be designated 4′-OMTs. Of the four proteins, ObFOMT4 has the most stringent regioselectivity, its 4′-*O*-methylating activity being negligible with all offered flavonoids except chrysoeriol (CHRYS; Fig. 1), an unlikely natural substrate.

Kinetic properties indicate LAD to be a better substrate than SCU7Me for ObFOMT4 and ObFOMT6 (Table II). The dimethylated substrate CIRM is also strongly preferred by ObFOMT3 over the monomethylated SCU7Me. Only ObFOMT5 kinetically prefers SCU7Me over CIRM. With sufficient SAM supply, the reactions easily proceed to full turnover, ruling out product inhibition. These properties imply that the abundance of SCU7Me might affect the relative abundances of three methylation products: CIRM, LAD, and SALV. As illustrated by Supplemental Figure S5, high amounts of SCU7Me favor higher relative abundances of CIRM and LAD when incubated with both ObFOMT3 and ObFOMT4. In the presence of lower concentrations of SCU7Me, CIRM and LAD outcompete it more easily and serve as preferred substrates, resulting in SALV as a major product.

An important regulatory mechanism to consider was inhibition of F6/4′OMTs by flavones that are poor or not substrates but are likely to occur in the cell. SALV was not a promising candidate because, as mentioned above, both ObFOMT4 and ObFOMT3 easily convert all supplied LAD and CIRM, respectively, into this common final product. Instead, we incubated ObFOMT4 with 5 μM LAD, its best substrate, and 5 μM CIRM, the flavone it produces from SCU7Me but does not methylate further. The yields of SALV only reached 73.7% of the uninhibited reaction, suggesting product inhibition by CIRM. This effect was not exerted by LAD in analogous experiments for ObFOMT3.

ObFOMT3 could also be the enzyme that forms API-diMe in vivo by 4′-methylation of GENK, even though it is not clear whether API-diMe originates from 4′- or 7-methylation as the first step (Table I). Kinetic analysis of this reaction revealed that GENK inhibits turnover at concentrations above 2.5 μM (substrate inhibition) and reaches half-maximal velocity at approximately 130 nM (Table II). ObFOMT5 behaves similarly, with substrate inhibition setting in at GENK concentrations above 10 μM.

A feature of all characterized F6/4′OMTs that distinguishes them from the F7OMTs and might prove important to physiological processes is the significantly lower affinity (relative to F7OMTs) for the cosubstrate, SAM, reflected by apparent K_m values

between 21 and 78 μM (Table II). We tested whether the SAM/SAH balance would affect the product profile by monitoring reactions with SCU7Me as substrate for ObFOMT3 and ObFOMT4 at 0, 25, or 50 μM SAH in the presence of 400 μM SAM. The relative abundances of the three products do change substantially as SAH concentrations change (Supplemental Fig. S6). Not surprisingly, the second methylation step, which relies on products formed in the first, is affected more than the first methylation of directly supplied SCU7Me. While EST and proteomics analyses of glandular trichomes from young leaves (Xie et al., 2008) clearly showed that the SAM cycle enzymes are among the most abundant in basil glandular trichome secretory cells, the SAM/SAH ratio may well be different in trichomes from the older leaves used in this analysis.

As a result of substrate screening, SCU7Me emerged as a good substrate for all FOMTs we characterized that were not F7OMTs. SCU7Me is also the latest possible common precursor for CIRM and LAD. Based on kinetic properties of the putatively involved OMTs, the abundance of SCU7Me might affect the relative abundances of CIRM, LAD, and SALV (see above), making it a key intermediate in the metabolism of 5,6,7,4′-hydroxylated flavones in basil. Metabolic routes passing through SCU7Me as a precursor of all higher methylated flavones are highly favored (Table I). Conversely, the turnover rates are much lower in the reaction sequence beginning with the 4′-*O*-methylation of API or SCU and including 7-*O*-methylation as the second step. The 7-*O*-methylation activities with 6-methoxylated substrates represented by HISP and nepetin (NEP; Fig. 1) are close to negligible. Therefore, it seems likely that the formation of both LAD and CIRM should proceed via a 7-*O*-methylation as the first step, which can occur either on SCU or on API, which is the best substrate of the F7OMTs.

Flavone Methylation in Basil Trichome Protein Extracts

Only non-cation-dependent FOMTs have been reported to methylate positions 7 and 4′ (Schröder et al., 2004; Willits et al., 2004), whereas earlier published studies of flavonoid 6-OMTs identified responsible proteins as SAM- and Mg^{2+}-dependent enzymes (De Luca and Ibrahim, 1985a; Ibdah et al., 2003). Such putative phenylpropanoid-flavonoid Mg^{2+}-dependent OMTs (Ibdah et al., 2003) are quite abundant in our EST database. However, our results revealed that several recombinant non-Mg^{2+}-dependent FOMTs can efficiently and selectively catalyze 6-*O*-methylation. To estimate the respective importance of these OMT classes in flavone metabolism, we compared the methylating activities of crude desalted trichome protein from lines SD and EMX-1 with and without Mg^{2+}. Such protein extracts were expected to comprise all or most of the FOMT activities present in the glands.

In these assays (Fig. 4A), SD protein extracts showed higher specific activities with all tested substrates.

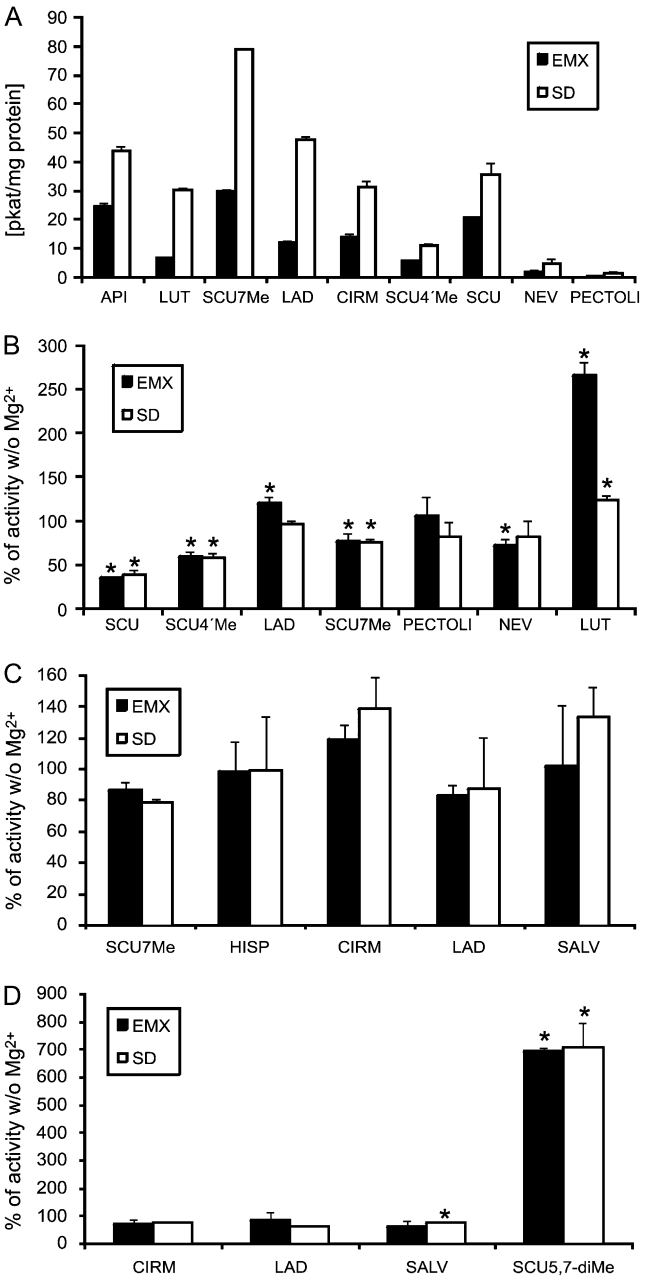

Figure 4. Flavone *O*-methylation activities in crude desalted protein extracts from isolated trichomes. A, Overview of activities with crude trichome protein as catalyst. Results are means ± SD ($n = 3$). B, Activities in the presence of Mg^{2+} relative to activities without cation addition. Assays with four potential substrates (SCU, SCU4′Me, LAD, and SCU7Me) for flavone 6-*O*-methyltransferase activity were conducted to check for Mg^{2+}-dependent OMTs and those with PECTOLI/NEV were conducted to demonstrate that F7OMT activities with these substrates are negligible with and without cation. Error bars indicate SD ($n = 3$). C and D, Methylation products in crude desalted protein extracts in the presence of Mg^{2+} relative to their abundances without cation addition and SCU (C) or SCU7Me (D) as substrate. Error bars indicate SD ($n = 2$). $^*P < 0.05$ (Student's unpaired two-tailed *t* test).

Highest turnover was measured with SCU7Me, consistent with our finding that it serves as an excellent substrate both for 6- and 4′-OMTs. Only low activity was detectable with NEV and virtually none with PECTOLI (Fig. 4, A and B). These two flavones have free 7-OH but methylated 6- and 4′-OH groups and are not readily methylated by the two F7OMTs we characterized (Table I). These results demonstrated that we have not failed to identify a divergent F7OMT that is specialized to accept these flavones. Instead, there is indeed only very low methylating activity toward both NEV and PECTOLI present in trichomes. This explains why NEV can accumulate in the trichomes and excludes PECTOLI and NEV as precursors of SALV and GARD B, respectively (Fig. 1).

To probe the effect of Mg^{2+} on 6-*O*-methylation by trichome proteins, we tested four potential substrates, SCU, SCU7Me, SCU4′Me, and LAD. Neither the total turnover rates (Fig. 4B) nor the formation rates of individual products with SCU and SCU7Me (Fig. 4, C and D) supported significant involvement of Mg^{2+}-dependent OMTs in 6-*O*-methylation. In fact, several reactions were inhibited by Mg^{2+} when crude protein from trichomes was used in assays but not when recombinant individual FOMTs were tested in vitro (Supplemental Table S3). This effect is likely due to other FOMTs present in the protein preparations used. Importantly, a third flavone with mass-to-charge ratio 315 in positive ionization mode was formed by crude protein extracts with SCU7Me as substrate. Judging by a previous report (Greenham et al., 2003) and considering our knowledge about other dimethylated SCU derivatives, it is likely to be SCU5,7-dimethyl ether, a compound never reported to occur in basil. This product was barely detectable in assays without Mg^{2+} and increased by over 700% upon addition of the cation, implying that it was formed by an Mg^{2+}-dependent OMT (Fig. 4D). The detection of this activity fortuitously provides an endogenous control for the inactivity of Mg^{2+}-dependent OMTs in assays lacking externally added cation. It also implies that the involvement of the latter OMT class in 6-*O*-methylation is negligible in basil. This reaction thus presents another example of convergent evolution in plants, where the same regioselectivity is exhibited by proteins belonging to two different enzyme families.

The Basis for the Distinct Regioselectivities of F6/4′OMTs

The high identity of the four ObF6/4′OMT proteins (see above) dictates that their differential regioselectivity is determined by differences in just a few specific amino acid residues. Therefore, these proteins offer a unique opportunity to study structural elements that define the regiospecificity and substrate specificity within a group of closely related enzymes.

The crystal structures of several non-Mg^{2+}-dependent OMTs have been solved (Zubieta et al., 2001, 2002; Liu et al., 2006; Louie et al., 2010), and all have similar overall fold and catalytic mechanisms (Noel et al., 2003). Basil FOMTs share the highest identity (30%–32%) and similarity (approximately 55%) to isoflavone 7-*O*-methyltransferase from alfalfa (*Medicago sativa*; IOMT [Protein Data Bank accession 1FP2]; Zubieta et al., 2001) compared with other OMTs with available structure data (Supplemental Fig. S7). Consequently, we used IOMT as a template for homology model construction.

The active sites of ObFOMT3 and ObFOMT4, as predicted by modeling, are slit shaped yet spacious enough to explain the acceptance of several different substrates, especially of planar molecules like the flavones (Fig. 5). As has been found for all OMTs of this class, the N terminus of the dyad-related monomer contributes to shaping the back wall of the substrate-binding site. In the case of basil FOMTs, the hydrophobic residues Trp-14 and Leu-18 will potentially accommodate the 7-OMe residue of SCU7Me when it is positioned for 4′-*O*-methylation. In addition, Leu-289 could contribute to the hydrophobic pocket. Tyr-20 can form an H-bond with the 5-OH of the flavone backbone in ObFOMT3. His-241 is very likely to act as the catalytic base (Zubieta et al., 2001, 2002). The overall shape of the active sites is identical in the three proteins (ObFOMT3–ObFOMT5) that we were most interested in.

One of our goals was to find a structural explanation for the stringent regioselectivity of ObFOMT4, whose activity is almost limited to 6-*O*-methylation, as opposed to ObFOMT3, which can act as either a 6- or 4′-OMT, depending on the substrate. The difference is most evident with SCU7Me, a potential key intermediate of flavone metabolism. ObFOMT3 preferentially acts as a 4′-OMT upon this substrate, while ObFOMT4 efficiently catalyzes only its 6-*O*-methylation. For the reactions to yield their respective products, SCU7Me has to be bound in opposite orientations. An analysis of the amino acid residues suggested by the models to line the substrate-binding site pointed out two residues of interest: Met-296 and Thr-292 in ObFOMT4, corresponding to Val-296 and Ile-292 in ObFOMT3 (Fig. 5). Met-296 of ObFOMT4 might extend into the binding cavity, leaving less space for the C-ring of flavones bound for 4′-*O*-methylation, thereby reducing the 4′-OMT activity. The mode of its interference with substrate binding could not be deduced from the model, and detailed crystallographic investigations will be required in order to determine just how Met-296 might be involved in restricting 4′-*O*-methylation. Thr-292 is positioned on the diagonally opposite side across from His-241, the probable catalytic base that deprotonates the acceptor hydroxyl group. This Thr can form a hydrogen bond with a 4′-OH group of SCU7Me or SCU, stabilizing its binding orientation for 6-*O*-methylation.

Interestingly, our EST database contains several minor contigs encoding the C-terminal OMT fragment that differs from ObFOMT3 by just this I292T mutation

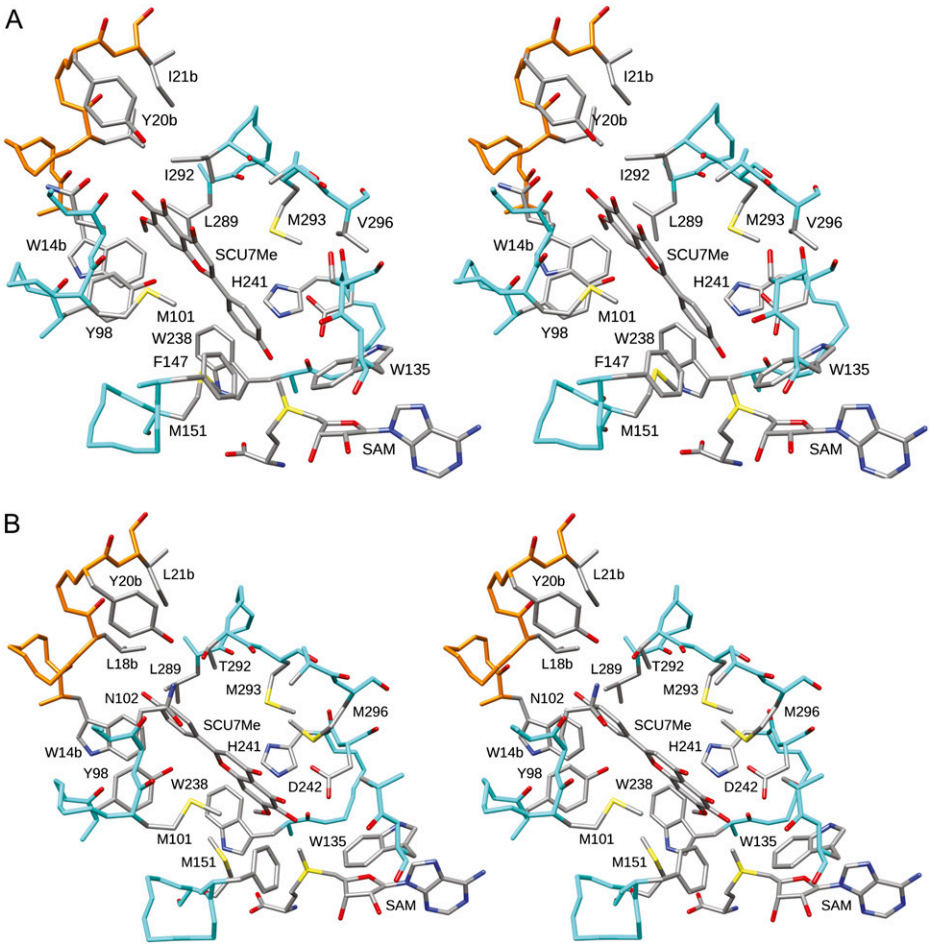

Figure 5. Active sites of ObFOMT3 (A) and ObFOMT4 (B) modeled with SAM and SCU7Me as ligands. Wall-eye views are presented. The SCU7Me ligands were placed in a position consistent with the observed activity before running Modeller. O4′ was positioned facing SAM in ObFOMT3, and O6 was positioned facing SAM in ObFOMT4. Backbone bonds for the chain in A are colored cyan, and backbone bonds for the chain in B are colored orange. Amino acid side chains are labeled where space allows.

(contigs basil_0688, basil_0489, and basil_0260). To assess the effect of this single amino acid substitution, we generated a single mutant of ObFOMT3, I292T. Its relative activities with our flavonoid substrate set indicated that the mutant was very similar to ObFOMT3 (Table I). Only the turnover with naringenin-7-methyl ether (NAR7Me) was significantly higher. However, LAD's portion of the total products decreases from 90% in ObFOMT3 to 70% in this single mutant (Fig. 6A, trace 2). Due to the high affinity of ObFOMT3 and presumably of its I292T mutant, the formed CIRM is rapidly converted into SALV as soon as its concentration in the assay is high enough to outcompete SCU7Me. Analogous behavior was displayed by the ObFOMT3 I292V mutant, confirming the effect of residue 292 on substrate orientation (76% LAD; Fig. 6A, trace 3).

The single I292T mutation did not affect the high activity of the protein with CIRM while, nevertheless, affecting the regioselectivity (Table I). In contrast, the double mutant of ObFOMT3, I292T/V296M, methylated CIRM at a much lower rate, in agreement with the steric inhibitory effect ascribed to Met-296, and the shift toward SCU7Me 6-*O*-methylation was even more pronounced (Fig. 6A, trace 4). The two divergent Thr residues following Met-296 in ObFOMT4 were the next mutation target. The triple mutant of ObFOMT3, I292T/V296M/M297T, yielded almost exclusively CIRM as product (Fig. 6A). Because the reciprocal triple mutant of ObFOMT4 did not produce significantly more LAD, we also carried out the fourth mutation, T298A in ObFOMT4 and the reverse in ObFOMT3. The product profile did not change visibly for ObFOMT3, but detectable amounts of LAD were formed by the ObFOMT4 mutant (Fig. 6A, traces 6 and 7). The fact that the activity with LAD of ObFOMT4 mutants did not decrease but remained comparable to that with SCU7Me as substrate (Supplemental Table S4) suggests that SALV formation by ObFOMT4 triple and quadruple mutants (visible in traces 8 and 7 of Fig. 6A) is due to the methylation of LAD produced in the first step from SCU7Me. In contrast, the reaction velocities with LAD increase gradually relative to those with SCU7Me as more mutations are introduced in ObFOMT3, reaching a maximum in the quadruple mutant (Supplemental Table S4).

The introduced mutations reduced reaction rates of ObFOMT3 and ObFOMT4 with SCU7Me. The activity of ObFOMT3 and ObFOMT4 quadruple mutants amounted to 1.71 and 0.75 nkat mg^{-1}, respectively, thus

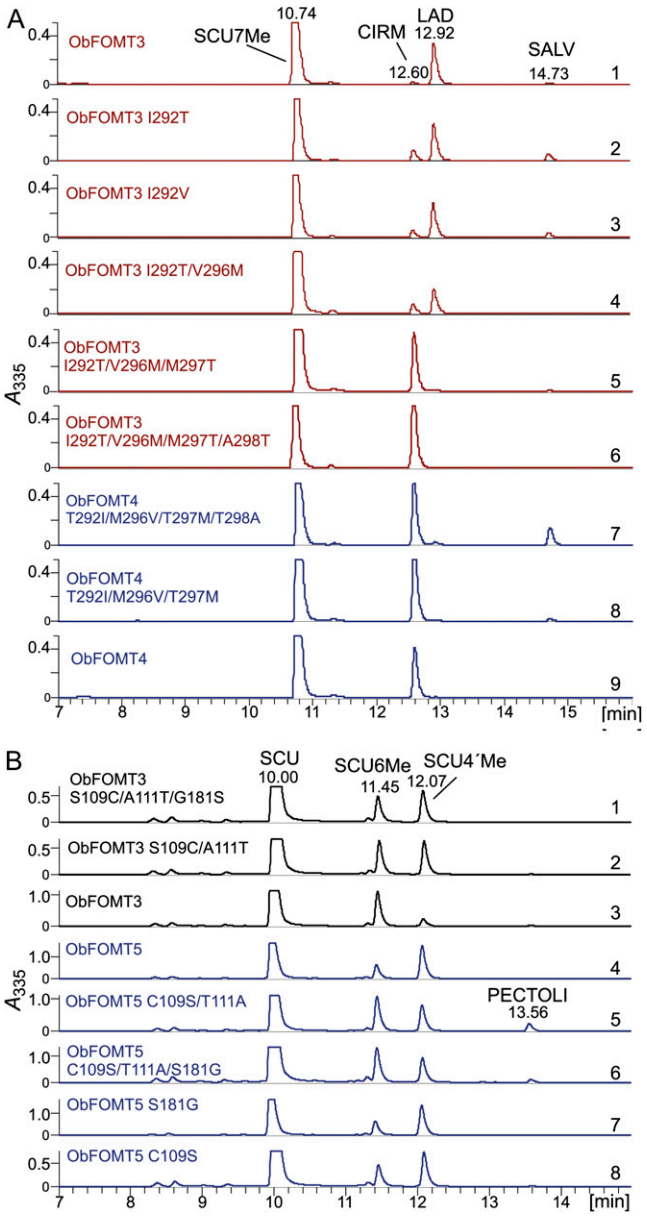

Figure 6. Identification of residues involved in the modulation of regioselectivities and therefore functional differentiation of basil FOMTs. Proteins and mutations are indicated on the left, and trace numbers as used in the text are on the right above the baseline. A, Effects of mutations on the 6- or 4′-*O*-regioselectivity of ObFOMT3 and ObFOMT4 with SCU7Me as substrate. B, Effect of mutations on the 6- or 4′-*O*-regioselectivity of ObFOMT3 and ObFOMT5 with SCU as substrate. [See online article for color version of this figure.]

being moderately or strongly decreased as compared with wild-type enzymes (Table I). Yet, the turnover rate of the ObFOMT3 quadruple mutant with LAD reached up to 3.08 nkat mg^{-1}, which exceeds the highest turnover rates found in ObFOMT3.

The second apparent difference between the F6/4′OMTs was illustrated by the product profiles with SCU (Supplemental Fig. S3A). It was most interesting to identify the structural elements that modulate the methylation of SCU by ObFOMT3 and ObFOMT5 toward dominance of HISP and SCU4′Me as respective products. The predicted flavone-binding sites of these two OMTs are conserved. This suggested that the different behaviors of these two proteins were caused by indirect effects on the proteins' conformation. The importance of the subunit interface in determining the shape of the substrate-binding site is a known feature of Mg^{2+}-independent OMTs (Noel et al., 2003). The models pointed out two residues (109 and 111) that are divergent in ObFOMT3 and ObFOMT5 and are also likely to affect the interaction between the subunits of the homodimer. Indeed, the product ratio of the C109S single mutant of ObFOMT5, and even more so of the C109S/T111A double mutant, shifted toward 6-methylation (Fig. 6B; Supplemental Table S5). Reciprocal mutations in corresponding positions of ObFOMT3 resulted in significantly increased formation of SCU4′Me.

Another divergent residue we tested was Ser-181 (Gly-181 in ObFOMT3), which, being part of the conserved signature SAM-binding motif (Ibrahim et al., 1998), could affect SAM binding and thus the shape of the substrate-binding pocket. We generated triple mutants for both ObFOMT5 and ObFOMT3. A comparison of the full substrate profiles for these triple mutants (positions 109, 111, and 181) revealed that their patterns became nearly identical to that of the reciprocal OMT (Table I). Most striking was the effect on the turnover with CIRM relative to SCU7Me, which was strongly increased in the ObFOMT5 C109S/T111A/S181G mutant and reduced in the reciprocal ObFOMT3 mutant. At the same time, the product profiles with SCU did not fully interchange. Both criteria (product profile with SCU and relative activities with SCU7Me/CIRM) indicate that residues 109 and 111 are primarily responsible for the achieved effects (Fig. 6B; Supplemental Table S5).

In summary, homology modeling-guided site-directed mutagenesis allowed us to identify important residues that strongly affect the 6- or 4′-regioselectivity by two distinct mechanisms: either by direct interaction in the substrate-binding site, as shown for the ObFOMT3 and ObFOMT4 comparison, or by indirectly modulating the shape of the active site, as in the case of the ObFOMT3 and ObFOMT5 comparison. In the latter case, the exact nature of the interactions cannot be predicted using modeling. Real crystallographic data will be necessary to reveal the actual substrate-binding modes in individual cases.

Flavone Profiling and FOMT Expression over a Developmental Time Course

To assess whether the FOMTs described above play the proposed roles in vivo, we evaluated the correlation between accumulated metabolites and individual gene expression. Analysis of directly collected oil

suggested that the flavones are predominantly localized to the subcuticular space of the peltate glands. However, transcript profiling required RNA isolation, which is not feasible using the glass capillary sampling technique. Therefore, we used whole leaf tissue as the source for metabolite and nucleic acid extraction. To recognize existing trends, we collected true leaf pairs of five plants of each line when they reached three-leaf-pair, five-leaf-pair, and seven-leaf-pair developmental stages. The youngest leaf pair (fourth, sixth, and eighth, respectively) was not analyzed because it would not yield enough material for both analyses.

The total flavone patterns are fairly conserved over the monitored time periods but exhibit some differences between the two basil lines (Fig. 7; Supplemental Fig. S8). For example, the concentrations of individual compounds increase steadily toward the youngest leaf in SD plants, while in EMX-1, the youngest leaf contains less flavones per gram fresh weight than the second youngest. In both lines, SALV is the major 8-unsubstituted flavone. Importantly, the amounts of SALV's precursors CIRM and LAD relative to total flavone accumulation were higher in EMX-1 (11%–18%) compared with SD (4%–11%) leaves; moreover, the content of LAD relative to CIRM was 7% to 12% higher in EMX-1. The relative concentration of API-diMe was nearly doubled in SD compared with EMX-1 but was generally less than 10% of the total flavone content. GENK is not shown in the diagrams but can be detected in most samples in slightly lower amounts than API-diMe. A peak with mass signal of mass-to-charge ratio 301 eluting at the retention time of SCU7Me, the preferred substrate for major basil F6/4′OMTs, is present in amounts of up to 1.5 μg g^{-1} fresh weight in numerous but not all samples. Evaluation of relative flavone amounts in successive leaves revealed a consistent increase toward the youngest leaves in both basil lines in SALV's proportion of the total flavone content (e.g. from 24.2% in the first leaf pair to 33.5% in the seventh leaf pair in line SD, and from 28.2% in the oldest leaf pair to 33.5% in the seventh leaf pair in EMX-1; Fig. 7). The older SD leaves contained more CIRM and LAD as a percentage of total flavone content (9.48% and 3.61%) than younger leaves (4.85% and 1.66%). The latter trend is not pronounced in EMX-1.

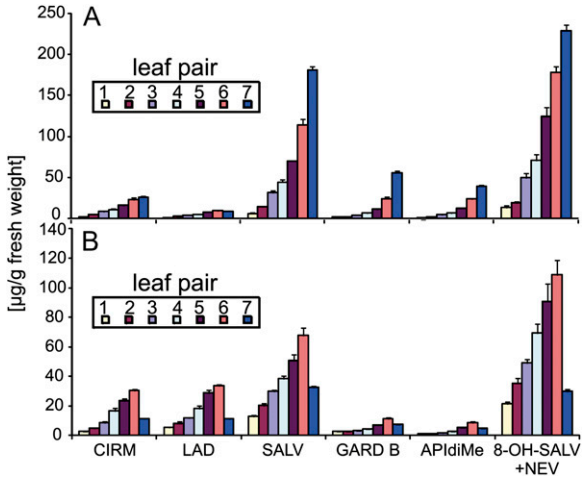

Figure 7. Accumulation of selected flavones in basil lines SD (A) and EMX-1 (B) at the seven-leaf-pair growth stage. The key indicates leaf number (1 is the oldest). Results are means of five biological replicates ± SE. [See online article for color version of this figure.]

The 8-substituted flavones detected were GARD B, PIL, NEV, and 8-OH-SALV. The relative concentration of GARD B was highest in youngest leaves, whereas PIL accumulation varied strongly between replicates. NEV and 8-OH-SALV were quantified as one compound due to separation difficulties. Their relative concentration increased by 11% to 15% toward older leaves in both basil lines. The opposite shifts in relative abundances of SALV and NEV/8-OH-SALV occur as the leaf expands and thus depend on leaf age. These shifts will probably be explained when we elucidate the underlying biosynthetic steps.

A comparison of corresponding leaf positions over the developmental time course suggests that total flavone content in mature leaves reaches a certain maximum after which production ceases. For example, the oldest leaves of EMX-1 and SD contain approximately 47 and 30 μg flavones g^{-1} fresh weight when the plants have five leaf pairs, which compares very well with 45 and 25 μg g^{-1} found in plants with seven leaf pairs (Fig. 7; Supplemental Fig. S8). Except for the youngest EMX-1 leaf pair, the flavone concentrations decrease in expanding leaves that are gaining fresh weight. For example, the flavone content in the fourth leaf pair of EMX-1 and SD decreases from 173 and 209 μg g^{-1} fresh weight at the five-leaf-pair stage to 144 and 149 μg g^{-1} at the seven-leaf-pair stage, respectively. Exclusive biosynthesis and accumulation of flavones in peltate glands that stop metabolic activity after their maturation provide the best explanation for this observation.

In order to estimate whether the studied FOMTs may indeed contribute to the differences in flavone profiles between the two basil lines, as well as between leaves of different ages in agreement with their biochemical properties, we analyzed their relative expression levels using quantitative reverse transcription-PCR in all leaf pairs of seven-leaf-pair stage plants. We were looking for subtle differences, since the flavone profiles are overall similar. Clearly, even though the same tissue was used for metabolite and gene expression analyses, the results of these experiments should be interpreted with caution, as transcript levels for selected genes may not reflect the overall enzymatic activities present in the glands. ObFOMT6, which is encoded by only two ESTs and has essentially the same activity as ObFOMT4, was not analyzed. The trends in FOMT expression were compared with those of flavone synthase (FNS), a core flavone metabolism gene whose expression in nontrichome leaf tissue is expected to be low to negligible (Grayer et al., 2002). Chalcone

synthase, the first committed enzyme of the flavonoid pathway, would be less suitable, as it is involved in leaf flavonoid glycoside biosynthesis. FNS transcript levels were highest in the youngest leaves and reached comparable levels in both lines (Fig. 8). The absence of correlation with the much lower flavone content of the youngest leaf pair of line EMX-1 (Fig. 7) suggests that FNS expression is not the key limiting factor for flavone accumulation. Indeed, the level of chalcone synthase expression/activity may exert control over the total flux (Knogge et al., 1986; Morreel et al., 2006). As mentioned above, monitoring the chalcone synthase transcripts in our experimental setup did not appear appropriate.

The expression levels of all five methyltransferases decreased as the leaves aged in both lines. Between the sixth and seventh leaf pair in line SD, the difference was 2- to 2.5-fold. This difference was even more pronounced in EMX-1 leaves, ranging between 3- and 5-fold. This result was not altogether surprising, since, as discussed above, the total amount of flavones is expected to be determined by the activity of core flavonoid pathway proteins. Overall, both FOMT and FNS expression levels drop dramatically as leaves get older. In agreement with metabolite accumulation data, this strongly implies that the localization of the external flavone production machinery is restricted to peltate glands, whose formation and maturation were earlier found to be completed long before the leaf reached its final size in basil (Werker et al., 1993).

The abundance of individual FOMT transcripts was generally higher in young SD leaves compared with EMX-1, except for ObFOMT5, whose expression levels were similar in both lines. The expression profiles of both F7OMTs that appear to be biochemically redundant did not provide any evidence of their specialization or complementary function. Interestingly, the differences between the F7OMT abundances in corresponding leaf pairs of the two lines were consistently lower (1.3- to 2.8-fold) than the differences in relative abundances of ObFOMT3 (2.4- to 6.4-fold) and ObFOMT4 (2.0- to 5.2-fold). Lower relative expression of the two major 6/4′-FOMTs in EMX-1 should favor higher relative amounts of LAD and CIRM in this line, agreeing with the metabolite data. The gene expression data also supported higher relative accumulation of LAD by line EMX-1 than by SD due to the already mentioned comparable expression level of ObFOMT5 and significantly lower abundances of ObFOMT3 and ObFOMT4. Whereas in SD, ObFOMT5 might be a less important player, in EMX-1, it is likely to contribute more noticeably to the conversion of SCU7Me into LAD. At the same time, the lower expression of ObFOMT4 in the same tissue results in slower turnover of LAD into SALV. In summary, keeping in mind the caveat stated above, the differences in metabolite profile appear to correlate with differential expression of appropriate FOMTs, which can be interpreted as strong evidence in support of their designated physiological functions.

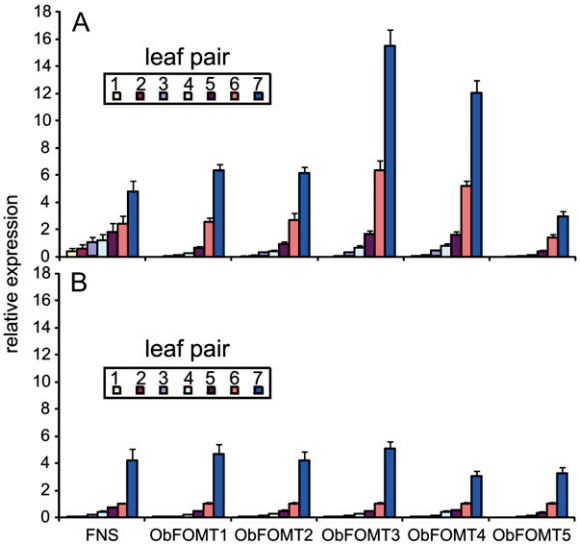

Figure 8. Transcript levels of ObFOMT1 to -5 and FNS in all leaf pairs of SD (A) and EMX-1 (B) plants at the seven-leaf-pair stage. Results are means of five biological replicates ± SE. For normalization and scaling, see "Materials and Methods." [See online article for color version of this figure.]

DISCUSSION

Functional Differentiation of Class II OMTs Contributes to Expansion and Fine-Tuning of Flavone Diversity in Sweet Basil

A phylogenetic analysis of the six basil methyltransferases (ObFOMT1–ObFOMT6) indicated that they belong to the "non-COMT" subfamily of the small molecule OMT class of *O*-methyltransferases (Gang et al., 2002; Noel et al., 2003; Gang, 2005) and form a clade with the peppermint F7- and F4′OMTs that is separate from other FOMTs (Fig. 3), suggesting a common origin. The peppermint F8OMT (Willits et al., 2004) and the putative basil F8OMT (b 0430), also members of the non-COMT subfamily, are more closely related to basil eugenol and chavicol OMTs than to F7- and F4′OMTs. The identities of the Lamiaceae FOMTs to OMTs from other families are below 45%, suggesting that the FOMT clade began to diverge long ago or has undergone rapid diversification. The identities between the F7OMTs and F4′OMTs from basil are around 51% to 53%, similar to what was found for FOMTs from peppermint (Willits et al., 2004). None of the basil contigs matches the peppermint F3′OMT (AAR09601) more closely than basil COMTs, whose function has been demonstrated previously (Gang et al., 2002). This could be due to lower expression of the underlying gene(s) or to catalysis of this reaction by a divergent enzyme.

It was not surprising that the basil F7OMTs and F4′OMTs are related to previously reported F7OMTs

and F4′OMTs that are also regioselective and non Mg^{2+} dependent (Schröder et al., 2004; Willits et al., 2004; Kim et al., 2005, 2006; Schmidt et al., 2011). In contrast, our finding that 6-*O*-methylation is largely engendered by a small family of F4′OMT-like, partly bifunctional class II small molecule OMTs in basil trichomes was rather unexpected, since both earlier studies regarding flavonoid (flavonol) 6-OMTs described Mg^{2+}-dependent enzymes (De Luca and Ibrahim, 1985a, 1985b; Ibdah et al., 2003).

While the preference for the 6-OH group as methyl acceptor is invariable in ObFOMT4, the regioselectivities of ObFOMT3 and ObFOMT5 are less stringent and depend on the offered substrate. Comparison of the respective products formed with a series of related flavones revealed that the 6-*O*-methylating activity observed toward SCU gave way to 4′-OMT activity when SCU7Me was offered as substrate instead, a phenomenon well explained by structural models. This means that the in vivo importance of ObFOMT3 and ObFOMT5 as 6-OMTs depends on the abundance of SCU as substrate, whereas in the presence of SCU7Me and CIRM, the preferred substrate of ObFOMT3, they function as flavone 4′-OMTs. We must reiterate that both proteins are also capable of 6-*O*-methylating LAD, whose 4′-OH is already methylated. Under cellular conditions, though, the 6-*O*-methylation of LAD will probably be carried out by ObFOMT4.

The high identity of the F6/4′OMTs suggests that they evolved via gene duplication, a well-known process in plant specialized metabolism. Mutagenesis experiments revealed that the change of regioselectivity from 4′- to 6-OMT can be achieved by a change in just three amino acid residues, whereas the reciprocal mutations did not result in a comparable activity shift. Thus, the 6-OMT activity could have evolved very rapidly and exerts, in its current specificity, a profound effect on the metabolic profile, enabling the production of CIRM from SCU7Me and strongly increasing the proportion of SALV, both by supplying CIRM for the F4′OMTs and by 6-*O*-methylating LAD. Its impact may reach to 8-substituted compounds if, as is to be expected, LAD, CIRM, or SALV is partitioned into that branch of the flavone network. Likewise, our results show that the functional separation of ObFOMT5 from ObFOMT3 requires very subtle structural changes. These are interesting conclusions that can be drawn from this study but that also warrant more detailed investigations in the future in order to further test these hypotheses.

Rapid change of activities is a known feature of OMTs (Wang and Pichersky, 1998, 1999; Frick and Kutchan, 1999; Gang et al., 2002; Scalliet et al., 2008; Bhuiya and Liu, 2010; Joe et al., 2010). The evolution of a new activity has been shown to result in the production of a specialized metabolite as compared with the core metabolic activity of the ancestor protein (Wang and Pichersky 1998) or production of a new specialized metabolite specific to a species/variety (Gang et al., 2002; Scalliet et al., 2008). Our results show how rapid functional differentiation of FOMTs was instrumental for the expansion of metabolic diversity within a growing network in one species. Similar processes are likely to occur in numerous other networks in other species.

The dedicated respective roles of ObFOMT1 to ObFOMT5 suggest that they can contain significant regulatory capacity, provided that they are indeed the major players involved. Obviously, 7-*O*-methylation is necessary for the supply of SCU7Me, a key substrate for 4′- and 6-OMTs. However, it is not likely to shape the metabolic profile but rather to act as a potential limiting factor for the production of methylated flavones. At the level of flavone profile definition, the design of the methylation processes in basil determines that changes in the expression of either of the two main F6/4′OMT genes will affect the accumulation of at least two compounds, the dimethylated and the trimethylated SCU derivatives. Large changes in the expression of either of these major genes would perturb the flavone profile. For instance, CIRM would be the major product and SALV would barely accumulate if the expression of ObFOMT3 were very low compared with ObFOMT4. Because of its lower efficiency with CIRM (Table II), the presence of ObFOMT5 would primarily affect the formation of LAD. Very high F4′/6OMT activities would favor the accumulation of SALV. Conversely, under conditions where the catalyst amounts are limiting, the relative abundance of these intermediates would be higher (Supplemental Fig. S5). In addition, the fact that none of the four F6/4′OMTs alone will as efficiently produce SALV from SCU7Me as in combination with a complementary OMT (e.g. ObFOMT3 with ObFOMT4) potentially contributes to the accumulation of CIRM and LAD, as these intermediates have to be transferred to a different protein for the next methylation step. In other words, both the abundance of individual FOMTs relative to each other as well as relative to enzymes upstream and downstream of the respective FOMT's position in the flavone biosynthetic network may exert regulatory effects on the flavone composition in different basil lines. Whether the regulation in planta truly can occur through titration of FOMT activities is a question that requires a suitable experimental system with variable methylation levels in order to be answered. In addition, the activities of minor contigs and their contribution to the metabolic profiles require investigation. Thus, this work has set the stage in developing hypotheses that now need to be tested regarding fundamental aspects of regulation of the flavonoid network in basil glandular trichomes.

One interesting aspect not addressed by this study is the possibility of heterodimer formation, which might further modulate the catalytic capacities of the FOMTs. It is well established that methyltransferases of this class typically function as homodimers (Noel et al., 2003). However, insect cells coexpressing combinations of four highly similar OMTs from *Thalictrum tuberosum* yielded products not formed by any of the

individual OMTs, clearly demonstrating that heterodimers were formed in vivo (Frick and Kutchan, 1999; Frick et al., 2001).

Line-Specific Profiles of External Flavones Are Conserved throughout Plant Development in Basil

The general flavone accumulation patterns seem to be conserved in basil lines, similar to flavone profiles in peppermint (Voirin et al., 1994). Monitoring the flavone composition at different plant growth stages indicated that it primarily depends on leaf age and not on the leaf's position on the stem. For example, we could observe a clear opposite shift of 10% to 15% in the relative abundances of SALV and NEV/8-OH-SALV (e.g. in the fifth leaf of both lines) analyzed at five- and seven-leaf-pair stages (Fig. 7; Supplemental Fig. S8). The shift is gradual, indicating that the underlying catalytic agents constitute the late phase of flavone metabolism, similar to menthone reductase and menthol acetyltransferase in essential oil production in peppermint (McConkey et al., 2000). Likewise, an opposite trend was observed in relative abundances of GARD B and pebrellin, a potential precursor of GARD B lacking only the 6-*O*-methyl group, which was attributed to changes in the expression of a F6OMT (Voirin and Bayet, 1992). This observation is in line with previous studies on terpene composition in basil (Johnson et al., 1999), peppermint (Brun et al., 1991), and thyme (*Thymus vulgare*; Yamaura et al., 1992) but contrasts with recent findings (Fischer et al., 2011) that the relative concentrations of several essential oil components in basil are strongly predetermined by the leaf position and vary little throughout leaf development.

Flavone accumulation patterns in successive leaf pairs at three plant development stages were typical of exclusive localization to glandular trichomes. The pattern is easy to recognize: the concentration of trichome-specific compounds is much higher in younger leaves that are still producing new epidermis cells and trichomes, and then the concentrations drop as the leaves expand. An important exception is represented by the youngest EMX-1 leaves. The flavone concentrations in this leaf pair were consistently lower than those in the second youngest leaf pair (Fig. 6; Supplemental Fig. S8). At the same time, the transcript levels of FOMTs and FNS followed the expected trichome-only pattern in both lines, including the youngest EMX-1 leaves (Fig. 7). So far, we have no data on whether FNS and FOMTs are induced by light. Yet, even if this were the case, the internode lengths between the top three leaves are so short that their respective light exposure is close to equal. This allows us to exclude light effects as the reason behind the metabolic and transcription patterns. The transcript pattern was also observed for chavicol and eugenol OMTs (Deschamps et al., 2006) that have been shown to be trichome specific (Gang et al., 2002). The discrepancy between the metabolite and transcript levels in the youngest EMX-1 leaf pair suggests flux limitation by a core phenylpropanoid/flavonoid pathway enzyme. While all leaves that we analyzed already contained significant amounts of flavonoids, none were detectable in extracts from peppermint leaves smaller than 2.5 mm in length (Voirin and Bayet, 1992), even though they already possess a considerable number of trichomes (Turner et al., 2000). Also, the concentrations of methylchavicol did not significantly increase in several younger leaf pairs of EMX-1 plants with six and eight leaf pairs (Deschamps et al., 2006). Potentially, there is a mechanism in both basil and peppermint that allows for the tight regulation of flavone/phenylpropanoid metabolism in young leaves and that is released more or less slowly in different lines/species, resulting in delayed accumulation of certain metabolites.

Biochemical Capacities Are Constrained by Multiple Cellular Factors in Defining the Line-Specific Flavone Profiles

In this work, we used combined approaches to gain insights into the metabolism of lipophilic flavones in basil trichomes as a model system. The same principles may apply to other species where similar compounds are produced by secretory structures. Detailed biochemical investigation of methylation processes led to the identification of a few superior, physiologically relevant substrates as well as highly favorable routes. The simplified network presented in Figure 1 points out the likely key intermediates, such as API and SCU7Me, the highly efficient metabolic conversions, such as the production of SALV both from CIRM and LAD (Table II), and several steps that will not occur, such as the late 7-*O*-methylations of PECTOLI and NEV (Table I; Fig. 4, A and B). In addition to directly addressed processes, we can make tentative predictions about steps we have not yet elucidated. For example, based on biochemical properties, API and not SCU is likely to be rapidly 7-*O*-methylated, making GENK a likely intermediate and a potential substrate for 6-hydroxylation by a currently unknown enzyme.

While the importance of the availability of catalytic capacities is self-evident, metabolic analyses provide hints that other factors are involved in defining the metabolic profile. For example, the accumulation of predicted intermediates LAD and CIRM alongside SALV in younger SD and EMX-1 leaves would not be expected, given the efficient methylation kinetics with both LAD and CIRM, the ample amounts of SAM as estimated by the abundance of SAM-salvage cycle transcripts and peptides (Gang et al., 2001; Xie et al., 2008), as well as the high expression and presumed activity of the involved FOMTs in the young tissue. In addition, we detected some discrepancies between the flavone composition in directly isolated oil versus leaf extracts, implying that certain flavones (e.g. CIRM, LAD, and PIL) could be distributed between several

compartments. Future quantitative analyses, especially with very few or individual trichomes, technology that is only now becoming available to us, will reveal what proportion of the total flavone amount remains in the secretory cells at different time points. Specific flavone profiles are likely to result, therefore, from enzyme capabilities, as well as the spatial and temporal colocalization of substrates/enzymes, transport for storage, and possible metabolon formation, as has been described for other metabolic networks (Jørgensen et al., 2005). Interestingly, basil FOMTs contain motifs that could indicate peroxisomal localization as an alternative to cytosol, as predicted by the PSORT server. The menthol pathway in peppermint trichomes is known to be highly compartmentalized (Turner and Croteau, 2004; Croteau et al., 2005). It is conceivable that the same applies to flavone metabolism in basil. Actual assessment of intracellular flavone transport, enzyme localizations, and metabolon formation will only become feasible after we complete the general elucidation of the biochemical network, as several central steps, such as 6- and 8-hydroxylations, are still obscure. While we have made an attempt to consider possible regulatory mechanisms, such as the effects that the abundances of the key substrate SCU7Me, other flavones, and SAH will exert (see "Results"), these experiments are limited at present by the lack of corresponding (sub)cellular metabolite profiling data. For example, detection of minuscule amounts of SCU7Me in leaf extracts does not exclude a high local short-term accumulation. On the other hand, accumulation of CIRM and LAD in the plant does not immediately mean that they are still located in the catalytically active compartment when we extract them. Indeed, from our analysis of flavones in the subcuticular cavity, it seems possible that rapid transport of intermediates (e.g. CIRM and LAD) into this compartment withdraws them from further metabolic processing. Importantly, the characterization of the menthol pathway in peppermint strongly suggests that transport into the oil cavity might not be unidirectional, as the conversion of menthone into menthol occurs in the late phase, after the secretion of menthone into the oil cavity (McConkey et al., 2000; Croteau et al., 2005). Thus, in addition to completion of biochemical studies, the identification and characterization of the transporters involved in intercellular and intracellular trafficking of these molecules will be a critical step in our efforts to understand how flavone metabolism is regulated in secretory tissue. A complete systems approach will likely be required to answer the important questions regarding the organization and regulation of the flavone metabolic network in basil glandular trichomes.

MATERIALS AND METHODS

Chemical Sources

S-Adenosyl-[^{14}C-methyl]-L-Met (48.8 mCi mmol^{-1}) was obtained from Perkin-Elmer. Unlabeled SAM was from Sigma-Aldrich. SCU, API, and LUT were purchased from Indofine; GENK, NEP, CHRYS, and acacetin (ACA) were from Extrasynthese. Cirsioliol (CIRL) was from Apin, diosmetin (DIOS) from Chromadex, and SCIN from Best Pharma Tech. CIRM and PECTOLI were obtained from TransMIT Biotech. Authentic samples of NEV, eupatorin (EUP), and GARD B were kindly donated by Dr. R. Grayer. Naringenin (NAR) and NAR7Me were a gift of Mark Berhow. LAD, SALV, SCU4′Me, and SCU7Me were partially synthesized using FOMTs described in this paper. Their exact preparation and purification procedures will be described elsewhere. Unless noted otherwise, laboratory supplies were of analytical quality and purchased from common vendors.

Plant Material Growth and Culture

Basil (*Ocimum basilicum*) seeds (lines EMX-1 and Sweet Dani) were germinated in vermiculite and individually repotted into SunGro mix. Plants were grown in growth chambers under a 16/8-h photoperiod and 28°C (24 h). Light intensity of approximately 200 μmol m^{-2} s^{-1} was supplied by incandescent and fluorescent lamps. Harvested plants were not returned to the growth chamber to avoid stress/wound signal transduction to still-growing plants.

Metabolite Extracts

Five solvent systems as well as five potential internal standards were compared in method optimization. The final procedure was as follows. Basil leaf pairs were ground under liquid nitrogen with a mortar and pestle. A portion of frozen powder was used for RNA extraction for transcript profiling (see below). Up to 200 mg of frozen powder was exactly weighed and suspended in 2 mL of methyl *tert*-butyl ether:ethyl acetate:ethanol (2:1:1, v/v/v) mix for metabolite analysis. A total of 100 μL of 125 μM 4-bromo-6-chloroflavone (Indofine) in ethyl acetate was added as an internal standard. After extraction overnight at room temperature under constant shaking, the suspension was centrifuged at 21,000*g* for 10 min at room temperature, the supernatant was carefully removed and stored at –20°C, and the remaining tissue was extracted overnight with 1 mL of solvent mix as above. Combined extracts were dried under a stream of nitrogen, and the dry residue was dissolved in 500 μL of ethyl acetate. An aliquot of 100 μL was again dried under nitrogen, and the residue was dissolved in 100 μL of 1:1 methanol: liquid chromatography (LC) buffer (5 mM ammonium formate, 0.1% formic acid) with 50 μM 8-anilino-1-naphthalene sulfonic acid (Sigma) as an internal standard. Five microliters of this final solution was injected for LC-mass spectrometry (MS) analysis.

Metabolite and Enzyme Assay Analyses

An LC-MS system (LCQ Advantage system with Surveyor HPLC and photodiode array detector; Thermo) was used to analyze flavones from basil whole leaf extracts prepared as described above. Metabolites were separated on a Discovery HS C_{18} column (150 × 2.1 mm, 3 μm; Supelco) kept at 40°C using a linear gradient of acetonitrile (B) and 5 mM ammonium formate-0.1% (v/v) formic acid buffer (A), 200 μL min^{-1}: 5% B in A for 2 min; 5% to 100% B in 53 min; 100% B for 5 min; 100% to 5% B in 2 min; column equilibration for 12 min. Positive mode electrospray ionization was applied for efficient ionization of polymethylated flavones. Tuning was carried out with API and API-diMe, resulting in similar ionization settings and efficiencies. Mass spectrometer settings were as follows: capillary at 275°C and 26 V, source 5.54 kV, sheath/sweep gas flow at 33/20. For collision-induced dissociation spectra, fragmentation was done using 45% to 55% normalized collision energy and either data-dependent or data-independent mode. Selected samples were also run on a Synapt G2 quadrupole-ion mobility spectrometry-time of flight mass spectrometer system (Waters) equipped with an Acquity UPLC system with photodiode array detector and an Acquity ultra performance liquid chromatography column (100 × 2.1 mm, 1.7 μm; Waters). The linear gradient was as above, except for flow rate of 400 μL min^{-1}: 0 min, 5% B; 0.86 min, 5% B; 9.69 min, 100% B; 10.52 min, 100% B; 11.02 min, 5% B; 13.02 min, 5% B. The Q-TOF-MS source was 3 kV at 130°C; desolvation temperature was 450°C; cone gas and desolvation gas flow were at 60 and 600 L h^{-1}, respectively. For MS^e fragmentation, the transfer collision energy was ramped between 25 and 45 eV. NAR was used for tuning, and calibration accuracy cutoff was 5 ppm. LeucineEnkephaline (accurate mass of 556.2771) was used for LockSpray. Quantification was based on standard curves produced using serial dilutions of authentic compounds. Comparison of UV_{335} and selected ion mass signals

of LAD and SALV with those of CIRM afforded quantification of the two former compounds.

Total RNA Extraction

To obtain RNA for cloning purposes, isolated glandular trichomes were disrupted by gentle sonication (2–3 × 10 s in a Branson 450 Sonifier equipped with a microtip; Branson Ultrasonics), and RNA was isolated using the RNeasy Plant Mini Kit (Qiagen) as described previously (Gang et al., 2001) with an intermediate on-column DNA digestion step of 30 min at ambient temperature using 10 units of RQ1 DNase (Promega).

Total RNA for quantitative PCR was extracted from ground leaves of different developmental stages using the RNeasy Plant Mini Kit (Qiagen). RNA was eluted with 35 μL of water, passed twice through the membrane to increase concentrations. To remove contaminating DNA, the eluates were treated with TURBO DNase (Ambion) in a final volume of 100 μL. Final RNA concentration was determined using Nanodrop 2000 (Thermo).

Trichome Protein Extraction and Enzyme Assays

Isolated glandular trichomes were disrupted and centrifuged at 8,000*g* and 4°C for 10 min to remove the debris. The supernatant was desalted through a PD-10 column (GE Healthcare) and eluted in 50 mM Tris-HCl, pH 7.5. Protein was measured according to Bradford (1976) using Bio-Rad reagent; a standard curve (bovine serum albumin) was used to calculate protein concentrations. Enzyme activities were measured either in radioactive assays or using unlabeled SAM followed by LC-MS analysis. Assays were processed and analyzed essentially as described below for recombinant proteins. Two to 10 μg of native trichome protein was supplied per reaction. The linearity of reaction at 30°C was verified with respect to protein amount and incubation time. Flavone concentration was 100 μM, radioactive SAM was supplied at 400 μM, and unlabeled SAM at 1 mM. Control assays contained solvent instead of flavone substrate or were quenched by 6 N HCl prior to starting the reaction. Controls and assays with PECTOLI and NEV were incubated for 60 min. All other assays were incubated for 10 to 30 min.

Isolation, Cloning, Site-Directed Mutagenesis, and Heterologous Expression of Basil FOMTs

To identify candidate genes, we searched the basil EST database (Gang et al., 2001) using the BLAST algorithm with peppermint (*Mentha* × *piperita*) 7-*O*- and 4′-*O*-FOMT sequences (Willits et al., 2004). Primers used to obtain full-length clones are shown in Supplemental Table S6, which were subcloned into pCR2.1 TOPO vector (Invitrogen) followed by transfer to pET15b (Novagen) for expression. Site-directed mutagenesis was carried out using the PCR method or QuikChange Lightning kit (Agilent); primer sequences are given in Supplemental Table S7. Expression in Rosetta 2 (DE3)pLysS cells (Novagen) with induction by 1 mM isopropyl-β-D-thiogalactoside was carried out overnight at 18°C to 20°C. Pelleted cells (3,000*g*, 4°C, 5 min) were suspended in binding buffer (50 mM potassium phosphate, 300 mM NaCl, pH 8.0, 5 mM imidazole, and 1% Tween 20) and disrupted by sonication. The clarified supernatant (15,000*g*, 4°C, 15 min) was loaded onto a nickel-nitrilotriacetic acid agarose matrix (Qiagen) that was preconditioned with the same buffer without Tween. The slurry was incubated for 1 h at 4°C under mild agitation. After washing with 8 volumes of washing buffer containing 20 mM imidazole, the proteins were eluted from the resin with buffer containing 250 mM imidazole, transferred into storage buffer (50 mM Tris-HCl, pH 7.5, 10% glycerol, and 1 mM dithiothreitol), and stored at –80°C.

Biochemical Characterization

For quantitative analyses, reaction conditions were chosen so that the reaction velocity was directly proportional to incubation time and protein amount. For kinetics measurements, saturating concentrations of the second substrate (flavone or SAM) were provided. Affinities for SAM were determined using API (ObFOMT1 and ObFOMT2), SCU (ObFOMT4), and CIRM (ObFOMT3 and ObFOMT5) as substrates. Kinetic parameters were derived from hyperbolic plots using nonlinear regression (Hyper.exe version 1.01; J.S. Easterby) and from classical linearization methods (e.g. Hanes).

The dependency of reaction rates on pH was determined in 50 mM sodium citrate-100 mM sodium phosphate buffer (pH 3.5–5.5), 100 mM potassium phosphate (pH 5.5–8.5), 50 mM Bis-Tris propane-HCl (pH 7.5–9.5), and 100 mM Gly-NaOH (pH 9.0–10.5). Tris, Bis-Tris, Bis-Tris propane, HEPES, TES, MES, and potassium phosphate at pH 7.0 were compared as buffer systems. Buffer concentrations were 100 mM except for Bis-Tris propane, which was 50 mM.

Radioactive assays were carried out in a total volume of 100 μL, stopped with 10 μL of 6 N HCl, and the products were extracted with 200 μL of ethyl acetate. After centrifugation for 3 min at 21,000*g*, an aliquot of the upper phase was added to 5 mL of Eco-Scint scintillation cocktail (National Diagnostics) and analyzed using a RackBeta 1215 scintillation counter (LKB). Relative reaction rates with a range of flavones were measured with 100 μM flavone and 100 μM SAM (ObFOMT1 and ObFOMT2), 200 μM SAM (ObFOMT3, ObFOMT3 I292V, and ObFOMT4), or 400 μM SAM (ObFOMT5 and ObFOMT6).

Unlabeled assays were carried out in a total volume of 100 μL under appropriate conditions, stopped with 10 μL of 6 N HCl, and the aqueous phase was extracted with 2 × 200 μL of ethyl acetate. After evaporating the combined organic phases, the dry residue was dissolved in 50 μL of 1:1 methanol:5 mM ammonium formate-0.1% formic acid LC buffer and analyzed using the LCQ or Synapt G2.

Sequence Similarity Analysis of Sweet Basil OMTs

Several BLAST searches against National Center for Biotechnology Information GenBank and basil EST database were conducted in order to collect currently known (putative) OMT sequences as comprehensively as possible. Contigs coding for all (putative) basil FOMTs as well as all other basil OMTs belonging to class II (Ibrahim et al., 1998) were collected. Duplicates (i.e. contigs encoding identical peptides) as well as peptides shorter than approximately one-third of the expected OMT length were removed. Resulting sequences were aligned using ClustalW version 2.1 at European Bioinformatics Institute (Larkin et al., 2007) with default settings. Sequence similarity relationships were inferred with MEGA5 (Tamura et al., 2011) using the neighbor-joining algorithm (Saitou and Nei, 1987) and 1,000 bootstrap replicates (Felsenstein, 1985). Distance calculation was done by Poisson correction. The tree was rooted using *Streptomyces anulatus O*-demethylpuromycin OMT as outgroup. Selected clusters were compressed for better overview. Accession numbers of the proteins in Figure 3 are given below. Full alignment of all used sequences can be found in Supplemental Data Set S1.

Quantitative PCR

A relative quantification method (Schmittgen and Livak, 2008) was used to assess the abundances of transcripts. Primers are listed in Supplemental Table S8. A detailed assay and method description can be found in Supplemental Materials and Methods S1. The *ELONGATION FACTOR1* gene served as a reference for normalization. For scaling, the relative expression of all genes in the sixth leaf pair of EMX-1 plants was set as 1. Five biological replicates of each leaf pair of both basil lines were analyzed.

Protein Structure Modeling

FOMT models were constructed using Modeller version 9 (Sali and Blundell, 1993) and IOMT from alfalfa (*Medicago sativa*; Protein Data Bank accession 1FP2; Zubieta et al., 2001) as the reference structure. The sequences for ObFOMT3 to -5 were simultaneously aligned to the sequence for the reference structure using ClustalW (Larkin et al., 2007). For each model, the sequence for the model and the reference structure were removed from the multialignment and used as input into modeler. The isoflavone ligand from the reference structure was converted to SCU7Me and repositioned with the program O (Jones, 1978). Models were viewed and rendered using UCSF Chimera (www.cgl.ucsf.edu/chimera).

Sequence data reported in this publication have been deposited in the GenBank/EMBL databases under the following accession numbers: ObFOMT1, JQ653275; ObFOMT2, JQ653276; ObFOMT3, JQ653277; ObFOMT4, JQ653278; ObFOMT5, JQ653279; ObFOMT6, JQ653280. The designations and accession numbers of proteins appearing in Figure 3 are as follows: *Streptomyces anulatus O*-demethylpuromycin OMT (outgroup), JQ1393ODPO; RcOMT3 (*Rosa chinensis* caffeic acid OMT), BAC78828; VvPyrOMT (*Vitis vinifera* hydroxypyrazine OMT, ADJ66850; HlOMT2 (*Humulus lupulus* OMT2), ABZ89566; HlDmxOMT (*H. lupulus* desmethoxyxanthohumol OMT), ABZ89565; EcRet7-OMT (*Eschscholzia californica* reticuline 7-OMT), BAE79723; CjColumbOMT

(*Coptis japonica* columbamine 2-OMT), BAC22084; ShF7/4′OMT (*Solanum habrochaites* myricetin 7/4′-OMT), ADZ76434; LnCA9OMT (*Linum nodiflorum* coniferyl alcohol 9-OMT), ABJ88947; ObEOMT (sweet basil eugenol OMT), AAL30424; ObCVOMT (sweet basil chavicol OMT), AAL30423; PpOMT (*Prunus pyrifolia* OMT), BAA86059; PaOMT (*Prunus armeniaca* OMT), AAB71213; PdOMT (*Prunus dulcis* OMT), CAA11131; HlOMT3 (*H. lupulus* OMT3), ABZ89567; peppermint MpF7OMTs, AAR09598 to AAR09599, MpF4′OMT, AAR09602; MpF8OMT, AAR09600; MpFOMT5, AAR09603; *Psychotria* spp. OMTs (compressed), BAI79243 to BAI79245; *Catharanthus* spp. OMTs (compressed), AAR02417, AAM97497 and -8, AAR02421, and AAR02419; IOMTs (isoflavonoid OMTs; compressed), AAC49856, BAC58011 to BAC58013, AAC49926, AAB88294, and Q29U70; alkaloid OMTs (compressed), AAP45313 to AAP45315, ACN88562, BAB08004, BAB08005, AAU20768, and AAU20765.

Supplemental Data

The following materials are available in the online version of this article.

Supplemental Figure S1. Comparison of flavone and rosmarinic acid accumulation in basil leaves versus subcuticular cavities of peltate trichomes.

Supplemental Figure S2. SDS-PAGE of affinity-purified basil FOMTs.

Supplemental Figure S3. Products of SCU and SCU7Me methylation by ObFOMT3 to -6 and selected mutants.

Supplemental Figure S4. Products of SCU methylation by ObFOMT3 to -6.

Supplemental Figure S5. Effect of starting SCU7Me concentration on products formed by a combination of ObFOMT3 and ObFOMT4.

Supplemental Figure S6. Effect of SAH on product profile formed by FOMT3 and FOMT4 from SCU7Me.

Supplemental Figure S7. Annotated alignment of ObFOMT3 to -6 with IOMT from alfalfa that was used as a template for homology modeling.

Supplemental Figure S8. Flavone profiles in successive leaf pairs of basil lines SD and EMX-1 at three- and five-leaf-pair development stages.

Supplemental Table S1. Percentage of identities between ObFOMT1 to -6.

Supplemental Table S2. Trivial, abbreviated, and International Union of Pure and Applied Chemistry names of flavonoids mentioned in this paper.

Supplemental Table S3. Basic characterization of ObFOMT1 to -6.

Supplemental Table S4. Relative activities of ObFOMT3 and ObFOMT4 mutants with SCU7Me, LAD, and CIRM.

Supplemental Table S5. Relative activities of ObFOMT3 and ObFOMT5 mutants with SCU, SCU7Me, and CIRM.

Supplemental Table S6. Primers used for full-length amplification of ObFOMT1 to -6.

Supplemental Table S7. Primers used for site-directed mutagenesis.

Supplemental Table S8. Primers used for quantitative PCR.

Supplemental Data Set S1. Full alignment of all sequences used for the construction of the neighbor-joining similarity tree in Figure 3.

Supplemental Materials and Methods S1. Analysis of gene expression by quantitative PCR.

ACKNOWLEDGMENTS

We thank Dr. R.J. Grayer (Royal Botanical Gardens) for authentic samples of NEV, GARD B, and EUP, Dr. Mark Berhow (U.S. Department of Agriculture-Agricultural Research Service) for authentic samples of NAR7Me and NAR, and the greenhouse staff of the Institute of Biological Chemistry, Washington State University, for raising the plants.

Received July 23, 2012; accepted August 23, 2012; published August 24, 2012.

LITERATURE CITED

Bhuiya M-W, Liu C-J (2010) Engineering monolignol 4-*O*-methyltransferases to modulate lignin biosynthesis. J Biol Chem **285:** 277–285

Bradford MM (1976) A rapid and sensitive method for the quantitation of microgram quantities of protein utilizing the principle of protein-dye binding. Anal Biochem **72:** 248–254

Brun N, Colson M, Perrin A, Voirin B (1991) Chemical and morphological studies of the effects of aging on monoterpene composition in *Mentha* × *piperita* leaves. Can J Bot **69:** 2271–2278

Clarke S, Banfield K (2001) *S*-Adenosylmethionine-dependent methyltransferases. *In* R Carmel, DW Jacobsen, eds, Homocysteine in Health and Disease. Cambridge University Press, Cambridge, pp 63–78

Cooper-Driver GA (1980) The role of flavonoids and related compounds in fern systematics. Bull Torrey Bot Club **107:** 116–127

Croteau RB, Davis EM, Ringer KL, Wildung MR (2005) (−)-Menthol biosynthesis and molecular genetics. Naturwissenschaften **92:** 562–577

De Luca V, Ibrahim RK (1985a) Enzymatic synthesis of polymethylated flavonols in *Chrysosplenium americanum*. I. Partial purification and some properties of S-adenosyl-L-methionine:flavonol 3-, 6-, 7-, and 4′-*O*-methyltransferases. Arch Biochem Biophys **238:** 596–605

De Luca V, Ibrahim RK (1985b) Enzymatic synthesis of polymethylated flavonols in *Chrysosplenium americanum*. II. Substrate interaction and product inhibition studies of flavonol 3-, 6-, and 4′-*O*-methyltransferases. Arch Biochem Biophys **238:** 606–618

Deschamps C, Gang D, Dudareva N, Simon JE (2006) Developmental regulation of phenylpropanoid biosynthesis in leaves and glandular trichomes of basil (*Ocimum basilicum* L.). Int J Plant Sci **167:** 447–454

Emerenciano VDP, Ferreira ZS, Kaplan MAC, Gottlieb OR (1987) A chemosystematic analysis of tribes of Asteraceae involving sesquiterpene lactones and flavonoids. Phytochemistry **26:** 3103–3115

Felsenstein J (1985) Confidence limits on phylogenies: an approach using the bootstrap. Evolution **39:** 783–791

Fischer R, Nitzan N, Chaimovitsh D, Rubin B, Dudai N (2011) Variation in essential oil composition within individual leaves of sweet basil (*Ocimum basilicum* L.) is more affected by leaf position than by leaf age. J Agric Food Chem **59:** 4913–4922

Frick S, Kutchan TM (1999) Molecular cloning and functional expression of O-methyltransferases common to isoquinoline alkaloid and phenylpropanoid biosynthesis. Plant J **17:** 329–339

Frick S, Ounaroon A, Kutchan TM (2001) Combinatorial biochemistry in plants: the case of *O*-methyltransferases. Phytochemistry **56:** 1–4

Gang DR (2005) Evolution of flavors and scents. Annu Rev Plant Biol **56:** 301–325

Gang DR, Lavid N, Zubieta C, Chen F, Beuerle T, Lewinsohn E, Noel JP, Pichersky E (2002) Characterization of phenylpropene *O*-methyltransferases from sweet basil: facile change of substrate specificity and convergent evolution within a plant *O*-methyltransferase family. Plant Cell **14:** 505–519

Gang DR, Wang JH, Dudareva N, Nam KH, Simon JE, Lewinsohn E, Pichersky E (2001) An investigation of the storage and biosynthesis of phenylpropenes in sweet basil. Plant Physiol **125:** 539–555

Grayer RJ, Bryan SE, Veitch NC, Goldstone FJ, Paton A, Wollenweber E (1996) External flavones in sweet basil, *Ocimum basilicum*, and related taxa. Phytochemistry **43:** 1041–1047

Grayer RJ, Kite GC, Abou-Zaid M, Archer LJ (2000) The application of atmospheric pressure chemical ionisation liquid chromatography-mass spectrometry in the chemotaxonomic study of flavonoids: characterisation of flavonoids from *Ocimum gratissimum* var. *gratissimum*. Phytochem Anal **11:** 257–267

Grayer RJ, Kite GC, Veitch NC, Eckert MR, Marin PD, Senanayake P, Paton AJ (2002) Leaf flavonoid glycosides as chemosystematic characters in *Ocimum*. Biochem Syst Ecol **30:** 327–342

Grayer RJ, Veitch NC, Kite GC, Price AM, Kokubun T (2001) Distribution of 8-oxygenated leaf-surface flavones in the genus *Ocimum*. Phytochemistry **56:** 559–567

Greenham J, Harborne JB, Williams CA (2003) Identification of lipophilic flavones and flavonols by comparative HPLC, TLC and UV spectral analysis. Phytochem Anal **14:** 100–118

Ibdah M, Zhang XH, Schmidt J, Vogt T (2003) A novel Mg(2+)-dependent O-methyltransferase in the phenylpropanoid metabolism of *Mesembryanthemum crystallinum*. J Biol Chem **278:** 43961–43972

Ibrahim RK, Bruneau A, Bantignies B (1998) Plant *O*-methyltransferases: molecular analysis, common signature and classification. Plant Mol Biol **36:** 1–10

Iijima Y, Davidovich-Rikanati R, Fridman E, Gang DR, Bar E, Lewinsohn E, Pichersky E (2004) The biochemical and molecular basis for the divergent patterns in the biosynthesis of terpenes and phenylpropenes in the peltate glands of three cultivars of basil. Plant Physiol **136:** 3724–3736

Joe EJ, Kim B-G, An B-C, Chong Y, Ahn J-H (2010) Engineering of flavonoid *O*-methyltransferase for a novel regioselectivity. Mol Cells **30:** 137–141

Johnson CB, Kirby J, Naxakis G, Pearson S (1999) Substantial UV-B-mediated induction of essential oils in sweet basil (*Ocimum basilicum* L.). Phytochemistry **51:** 507–510

Jones TA (1978) A graphics model building and refinement system for macromolecules. J Appl Cryst **11:** 268–272

Jørgensen K, Rasmussen AV, Morant M, Nielsen AH, Bjarnholt N, Zagrobelny M, Bak S, Møller BL (2005) Metabolon formation and metabolic channeling in the biosynthesis of plant natural products. Curr Opin Plant Biol **8:** 280–291

Kapteyn J, Qualley AV, Xie Z, Fridman E, Dudareva N, Gang DR (2007) Evolution of cinnamate/p-coumarate carboxyl methyltransferases and their role in the biosynthesis of methylcinnamate. Plant Cell **19:** 3212–3229

Kim B-G, Kim H, Hur H-G, Lim Y, Ahn J-H (2006) Regioselectivity of 7-*O*-methyltransferase of poplar to flavones. J Biotechnol **126:** 241–247

Kim DH, Kim BG, Lee Y, Ryu JY, Lim Y, Hur HG, Ahn JH (2005) Regiospecific methylation of naringenin to ponciretin by soybean *O*-methyltransferase expressed in *Escherichia coli*. J Biotechnol **119:** 155–162

Knogge W, Schmelzer E, Weissenböck G (1986) The role of chalcone synthase in the regulation of flavonoid biosynthesis in developing oat primary leaves. Arch Biochem Biophys **250:** 364–372

Larkin MA, Blackshields G, Brown NP, Chenna R, McGettigan PA, McWilliam H, Valentin F, Wallace IM, Wilm A, Lopez R, et al (2007) Clustal W and Clustal X version 2.0. Bioinformatics **23:** 2947–2948

Liu C-J, Deavours BE, Richard SB, Ferrer J-L, Blount JW, Huhman D, Dixon RA, Noel JP (2006) Structural basis for dual functionality of isoflavonoid *O*-methyltransferases in the evolution of plant defense responses. Plant Cell **18:** 3656–3669

Louie GV, Bowman ME, Tu Y, Mouradov A, Spangenberg G, Noel JP (2010) Structure-function analyses of a caffeic acid *O*-methyltransferase from perennial ryegrass reveal the molecular basis for substrate preference. Plant Cell **22:** 4114–4127

Maffei M, Chialva F, Sacco T (1989) Glandular trichomes and essential oil in developing peppermint leaves. New Phytol **111:** 707–716

McConkey ME, Gershenzon J, Croteau RB (2000) Developmental regulation of monoterpene biosynthesis in the glandular trichomes of peppermint. Plant Physiol **122:** 215–224

Morreel K, Goeminne G, Storme V, Sterck L, Ralph J, Coppieters W, Breyne P, Steenackers M, Georges M, Messens E, et al (2006) Genetical metabolomics of flavonoid biosynthesis in Populus: a case study. Plant J **47:** 224–237

Noel JP, Dixon RA, Pichersky E, Zubieta C, Ferrer JL (2003) Structural, functional, and evolutionary basis for methylation of plant small molecules. Recent Adv Phytochem **37:** 37–58

Pichersky E, Lewinsohn E (2011) Convergent evolution in plant specialized metabolism. Annu Rev Plant Biol **62:** 549–566

Roje S (2006) S-Adenosyl-L-methionine: beyond the universal methyl group donor. Phytochemistry **67:** 1686–1698

Saitou N, Nei M (1987) The neighbor-joining method: a new method for reconstructing phylogenetic trees. Mol Biol Evol **4:** 406–425

Sali A, Blundell TL (1993) Comparative protein modelling by satisfaction of spatial restraints. J Mol Biol **234:** 779–815

Scalliet G, Piola F, Douady CJ, Réty S, Raymond O, Baudino S, Bordji K, Bendahmane M, Dumas C, Cock JM, et al (2008) Scent evolution in Chinese roses. Proc Natl Acad Sci USA **105:** 5927–5932

Schmidt A, Li C, Shi F, Jones AD, Pichersky E (2011) Polymethylated myricetin in trichomes of the wild tomato species *Solanum habrochaites* and characterization of trichome-specific 3′/5′- and 7/4′-myricetin *O*-methyltransferases. Plant Physiol **155:** 1999–2009

Schmittgen TD, Livak KJ (2008) Analyzing real-time PCR data by the comparative C(T) method. Nat Protoc **3:** 1101–1108

Schröder G, Wehinger E, Lukacin R, Wellmann F, Seefelder W, Schwab W, Schröder J (2004) Flavonoid methylation: a novel 4′-*O*-methyltransferase from *Catharanthus roseus*, and evidence that partially methylated flavanones are substrates of four different flavonoid dioxygenases. Phytochemistry **65:** 1085–1094

Tamura K, Peterson D, Peterson N, Stecher G, Nei M, Kumar S (2011) MEGA5: molecular evolutionary genetics analysis using maximum likelihood, evolutionary distance, and maximum parsimony methods. Mol Biol Evol **28:** 2731–2739

Turner GW, Croteau R (2004) Organization of monoterpene biosynthesis in *Mentha*: immunocytochemical localizations of geranyl diphosphate synthase, limonene-6-hydroxylase, isopiperitenol dehydrogenase, and pulegone reductase. Plant Physiol **136:** 4215–4227

Turner GW, Gershenzon J, Croteau RB (2000) Distribution of peltate glandular trichomes on developing leaves of peppermint. Plant Physiol **124:** 655–664

Vieira RF, Grayer RJ, Paton AJ (2003) Chemical profiling of *Ocimum americanum* using external flavonoids. Phytochemistry **63:** 555–567

Voirin B, Bayet C (1992) Developmental variations in leaf flavonoid aglycones of *Mentha* × *piperita*. Phytochemistry **31:** 2299–2304

Voirin B, Bayet C, Colson M (1993) Demonstration that flavone aglycones accumulate in the peltate glands of *Mentha* × *piperita* leaves. Phytochemistry **34:** 85–87

Voirin B, Saunois A, Bayet C (1994) Free flavonoid aglycones from *Mentha* × *piperita*: developmental, chemotaxonomical and physiological aspects. Biochem Syst Ecol **22:** 95–99

Wang J, Pichersky E (1999) Identification of specific residues involved in substrate discrimination in two plant *O*-methyltransferases. Arch Biochem Biophys **368:** 172–180

Wang JH, Pichersky E (1998) Characterization of *S*-adenosyl-L-methionine: (iso)eugenol *O*-methyltransferase involved in floral scent production in *Clarkia breweri*. Arch Biochem Biophys **349:** 153–160

Werker E, Putievsky E, Ravid U, Dudai N, Katzir I (1993) Glandular hairs and essential oil in developing leaves of *Ocimum basilicum* L. (Lamiaceae). Ann Bot (Lond) **71:** 43–50

Willits MG, Giovanni M, Prata RTN, Kramer CM, De Luca V, Steffens JC, Graser G (2004) Bio-fermentation of modified flavonoids: an example of in vivo diversification of secondary metabolites. Phytochemistry **65:** 31–41

Wink M (2008) Plant secondary metabolism: diversity, function and its evolution. Nat Prod Commun **3:** 1205–1216

Wollenweber E (1989) Exudate flavonoids in ferns and their chemosystematic implication. Biochem Syst Ecol **17:** 141–144

Wollenweber E, Dietz VH (1981) Occurrence and distribution of free flavonoid aglycones in plants. Phytochemistry **20:** 869–932

Xaasan CC, Ciilmi CX, Faarax MX, Passannanti S, Piozzi F, Paternostro M (1980) Unusual flavones from *Ocimum canum*. Phytochemistry **19:** 2229–2230

Xie Z, Kapteyn J, Gang DR (2008) A systems biology investigation of the MEP/terpenoid and shikimate/phenylpropanoid pathways points to multiple levels of metabolic control in sweet basil glandular trichomes. Plant J **54:** 349–361

Yamaura T, Tanaka S, Tabata M (1992) Localization of the biosynthesis and accumulation of monoterpenoids in glandular trichomes of thyme. Planta Med **58:** 153–158

Zubieta C, He XZ, Dixon RA, Noel JP (2001) Structures of two natural product methyltransferases reveal the basis for substrate specificity in plant *O*-methyltransferases. Nat Struct Biol **8:** 271–279

Zubieta C, Kota P, Ferrer JL, Dixon RA, Noel JP (2002) Structural basis for the modulation of lignin monomer methylation by caffeic acid/5-hydroxyferulic acid 3/5-*O*-methyltransferase. Plant Cell **14:** 1265–1277